FERMILAB-PUB-24-0383-PPD

Evidence for large baryonic feedback at low and intermediate redshifts from kinematic Sunyaev-Zel'dovich observations with ACT and DESI photometric galaxies

B. Hadzhiyska,[1,2,3,*] S. Ferraro,[2,3] B. Ried Guachalla,[4,5,6] E. Schaan,[5,6] J. Aguilar,[7] S. Ahlen,[8] N. Battaglia,[9] J. R. Bond,[10] D. Brooks,[11] E. Calabrese,[12] S. K. Choi,[13] T. Claybaugh,[7] W. R. Coulton,[14,15] K. Dawson,[16] M. Devlin,[17] B. Dey,[18] P. Doel,[11] A. J. Duivenvoorden,[19] J. Dunkley,[20,21] G. S. Farren,[15,14] A. Font-Ribera,[11,22] J. E. Forero-Romero,[23,24] P. A. Gallardo,[25] E. Gaztañaga,[26,27,28] S. Gontcho Gontcho,[7] M. Gralla,[29] L. Le Guillou,[30] G. Gutierrez,[31] J. Guy,[7] J. C. Hill,[32] R. Hložek,[33,34] K. Honscheid,[35,36,37] S. Juneau,[38] R. Kehoe,[39] T. Kisner,[7] A. Kremin,[7] M. Landriau,[7] R. H. Liu,[3] T. Louis,[40] N. MacCrann,[15] A. de Macorra,[41] M. Madhavacheril,[17] M. Manera,[42,22] A. Meisner,[38] R. Miquel,[43,22] K. Moodley,[44] J. Moustakas,[45] T. Mroczkowski,[46] S. Naess,[47] J. Newman,[18] M. D. Niemack,[48] G. Niz,[49,50] L. Page,[20] N. Palanque-Delabrouille,[51,7] B. Partridge,[52] W. J. Percival,[53,54,55] F. Prada,[56] F. J. Qu,[15,14,5] G. Rossi,[57] E. Sanchez,[58] D. Schlegel,[7] M. Schubnell,[59,60] N. Sehgal,[61] H. Seo,[62] C. Sifón,[63] D. Spergel,[64] D. Sprayberry,[38] S. Staggs,[20] G. Tarlé,[60] C. Vargas,[65] E. M. Vavagiakis,[66] B. A. Weaver,[38] E. J. Wollack,[67] R. Zhou,[2] and H. Zou[68]

[1] *Miller Institute for Basic Research in Science, University of California, Berkeley, CA, 94720, USA*
[2] *Physics Division, Lawrence Berkeley National Laboratory, Berkeley, CA 94720, USA*
[3] *Berkeley Center for Cosmological Physics, Department of Physics, University of California, Berkeley, CA 94720, USA*
[4] *Department of Physics, Stanford University, Stanford, CA, USA 94305-4085*
[5] *Kavli Institute for Particle Astrophysics and Cosmology, 382 Via Pueblo Mall Stanford, CA 94305-4060, USA*
[6] *SLAC National Accelerator Laboratory 2575 Sand Hill Road Menlo Park, California 94025, USA*
[7] *Lawrence Berkeley National Laboratory, 1 Cyclotron Road, Berkeley, CA 94720, USA*
[8] *Physics Dept., Boston University, 590 Commonwealth Avenue, Boston, MA 02215, USA*
[9] *Department of Astronomy, Cornell University, Ithaca, NY 14853, USA*
[10] *Canadian Institute for Theoretical Astrophysics, Toronto, Ontario M5S 3H8, Canada*
[11] *Department of Physics & Astronomy, University College London, Gower Street, London, WC1E 6BT, UK*
[12] *School of Physics and Astronomy, Cardiff University, The Parade, Cardiff, Wales CF24 3AA, UK*
[13] *Department of Physics and Astronomy, University of California, Riverside, CA 92521, USA*
[14] *Kavli Institute for Cosmology Cambridge, Madingley Road, Cambridge CB3 0HA, UK*
[15] *DAMTP, Centre for Mathematical Sciences, University of Cambridge, Wilberforce Road, Cambridge CB3 OWA, UK*
[16] *Department of Physics and Astronomy, The University of Utah, 115 South 1400 East, Salt Lake City, UT 84112, USA*
[17] *Department of Physics and Astronomy, University of Pennsylvania, 209 South 33rd Street, Philadelphia, PA, USA 19104*
[18] *Department of Physics & Astronomy and Pittsburgh Particle Physics, Astrophysics, and Cosmology Center (PITT PACC), University of Pittsburgh, 3941 O'Hara Street, Pittsburgh, PA 15260, USA*
[19] *Center for Computational Astrophysics, Flatiron Institute, New York, NY 10010, USA, Joseph Henry Laboratories of Physics, Jadwin Hall, Princeton University, Princeton, NJ, USA 08544*
[20] *Joseph Henry Laboratories of Physics, Jadwin Hall, Princeton University, Princeton, NJ, USA 08544*
[21] *Department of Astrophysical Sciences, Princeton University, Peyton Hall, Princeton, NJ 08544, USA*
[22] *Institut de Física d'Altes Energies (IFAE), The Barcelona Institute of Science and Technology, Campus UAB, 08193 Bellaterra Barcelona, Spain*
[23] *Departamento de Física, Universidad de los Andes, Cra. 1 No. 18A-10, Edificio Ip, CP 111711, Bogotá, Colombia*
[24] *Observatorio Astronómico, Universidad de los Andes, Cra. 1 No. 18A-10, Edificio H, CP 111711 Bogotá, Colombia*
[25] *Kavli Institute for Cosmological Physics, University of Chicago, Chicago, IL, 60637, USA*
[26] *Institut d'Estudis Espacials de Catalunya (IEEC), 08034 Barcelona, Spain*
[27] *Institute of Cosmology and Gravitation, University of Portsmouth, Dennis Sciama Building, Portsmouth, PO1 3FX, UK*
[28] *Institute of Space Sciences, ICE-CSIC, Campus UAB, Carrer de Can Magrans s/n, 08913 Bellaterra, Barcelona, Spain*
[29] *Steward Observatory/Department of Astronomy, University of Arizona, Tucson, AZ 85721 USA*
[30] *Sorbonne Université, CNRS/IN2P3, Laboratoire de Physique Nucléaire et de Hautes Energies (LPNHE), FR-75005 Paris, France*
[31] *Fermi National Accelerator Laboratory, PO Box 500, Batavia, IL 60510, USA*
[32] *Department of Physics, Columbia University, New York, NY 10027, USA*
[33] *Department of Astronomy and Astrophysics, University of Toronto, 50 St. George Street, Toronto, ON M5S 3H4, Canada*
[34] *Dunlap Institute for Astronomy and Astrophysics, University of Toronto, 50 St. George Street, Toronto, ON M5S 3H4, Canada*
[35] *Center for Cosmology and AstroParticle Physics, The Ohio State University, 191 West Woodruff Avenue, Columbus, OH 43210, USA*
[36] *Department of Physics, The Ohio State University, 191 West Woodruff Avenue, Columbus, OH 43210, USA*

[37]The Ohio State University, Columbus, 43210 OH, USA
[38]NSF NOIRLab, 950 N. Cherry Ave., Tucson, AZ 85719, USA
[39]Department of Physics, Southern Methodist University, 3215 Daniel Avenue, Dallas, TX 75275, USA
[40]Université Paris-Saclay, CNRS/IN2P3, IJCLab, 91405 Orsay, France
[41]Instituto de Física, Universidad Nacional Autónoma de México, Cd. de México C.P. 04510, México
[42]Departament de Física, Serra Húnter, Universitat Autònoma de Barcelona, 08193 Bellaterra (Barcelona), Spain
[43]Institució Catalana de Recerca i Estudis Avançats, Passeig de Lluís Companys, 23, 08010 Barcelona, Spain
[44]Astrophysics Research Centre, School of Mathematics, Statistics and Computer Science, University of KwaZulu-Natal, Durban 4001, South Africa
[45]Department of Physics and Astronomy, Siena College, 515 Loudon Road, Loudonville, NY 12211, USA
[46]European Southern Observatory, Karl-Schwarzschild-Str. 2, Garching 85748, Germany
[47]Institute for theoretical astrophysics, University of Oslo, Norway
[48]Cornell University Physics Department, Cornell University, Ithaca, NY 14853, USA; Cornell University Astronomy Department, Cornell University, Ithaca, NY 14853, USA
[49]Departamento de Física, Universidad de Guanajuato - DCI, C.P. 37150, Leon, Guanajuato, México
[50]Instituto Avanzado de Cosmología A. C., San Marcos 11 - Atenas 202. Magdalena Contreras, 10720. Ciudad de México, México
[51]IRFU, CEA, Université Paris-Saclay, F-91191 Gif-sur-Yvette, France
[52]Department of Physics and Astronomy, Haverford College, Haverford PA 19041 USA
[53]Department of Physics and Astronomy, University of Waterloo, 200 University Ave W, Waterloo, ON N2L 3G1, Canada
[54]Perimeter Institute for Theoretical Physics, 31 Caroline St. North, Waterloo, ON N2L 2Y5, Canada
[55]Waterloo Centre for Astrophysics, University of Waterloo, 200 University Ave W, Waterloo, ON N2L 3G1, Canada
[56]Instituto de Astrofísica de Andalucía (CSIC), Glorieta de la Astronomía, s/n, E-18008 Granada, Spain
[57]Department of Physics and Astronomy, Sejong University, Seoul, 143-747, Korea
[58]CIEMAT, Avenida Complutense 40, E-28040 Madrid, Spain
[59]Department of Physics, University of Michigan, Ann Arbor, MI 48109, USA
[60]University of Michigan, Ann Arbor, MI 48109, USA
[61]Physics and Astronomy Department, Stony Brook University, Stony Brook, NY 11794
[62]Department of Physics & Astronomy, Ohio University, Athens, OH 45701, USA
[63]Instituto de Física, Pontificia Universidad Católica de Valparaíso, Casilla 4059, Valparaíso, Chile
[64]Center for Computational Astrophysics, Flatiron Institute, 162 5th Avenue, New York, NY 10010, USA
[65]Instituto de Astrofísica and Centro de Astro-Ingeniería, Facultad de Física, Pontificia Universidad Católica de Chile, Av. Vicuña Mackenna 4860, 7820436 Macul, Santiago, Chile
[66]Department of Physics, Duke University, Durham, NC 27708, USA; Department of Physics, Cornell University, Ithaca, NY 14853, USA
[67]NASA/Goddard Space Flight Center, Greenbelt, MD 20771, USA
[68]National Astronomical Observatories, Chinese Academy of Sciences, A20 Datun Rd., Chaoyang District, Beijing, 100012, P.R. China

(Dated: July 11, 2024)

Recent advances in cosmological observations have provided an unprecedented opportunity to investigate the distribution of baryons relative to the underlying matter. In this work, we robustly show that the gas is much more extended than the dark matter at 40σ and the amount of baryonic feedback at $z \lesssim 1$ strongly disfavors low-feedback models such as that of state-of-the-art hydrodynamical simulation IllustrisTNG compared with high-feedback models such as that of the original Illustris simulation. This has important implications for bridging the gap between theory and observations and understanding galaxy formation and evolution. Furthermore, a better grasp of the baryon-dark matter link is critical to future cosmological analyses, which are currently impeded by our limited knowledge of baryonic feedback. Here, we measure the kinematic Sunyaev-Zel'dovich (kSZ) effect from the Atacama Cosmology Telescope (ACT), stacked on the luminous red galaxy (LRG) sample of the Dark Energy Spectroscopic Instrument (DESI) imaging survey. This is the first analysis to use photometric redshifts for reconstructing galaxy velocities. Due to the large number of galaxies comprising the DESI imaging survey, this is the highest signal-to-noise stacked kSZ measurement to date: we detect the signal at 13σ and find that the gas is more spread out than the dark matter at $\sim 40\sigma$. Our work opens up the possibility to recalibrate large hydrodynamical simulations using the kSZ effect. In addition, our findings point towards a way of alleviating inconsistencies between weak lensing surveys and cosmic microwave background (CMB) experiments such as the 'low S_8' tension, and shed light on long-standing enigmas in astrophysics such as the 'missing baryon' problem.

* boryanah@alumni.princeton.edu

I. INTRODUCTION

Baryons, though comprising more than 15% of the universe's total matter content, continue to elude precise mapping in relation to the underlying dark matter [1]. This poses a significant challenge for the next generation of large-scale structure experiments, especially those measuring weak lensing, including the Vera Rubin Observatory [2, 3], Euclid [4], and the Nancy Grace Roman Space Telescope [5].

Realizing the full potential of these surveys necessitates subpercent-level knowledge of baryonic effects on cosmological observables. Furthermore, unraveling the astrophysical processes governing baryons within galaxies and galaxy clusters holds the key to deciphering the mysteries of galaxy formation and evolution. The bulk of baryons reside in the circumgalactic medium (CGM) and the intracluster medium (ICM), the baryon abundance and composition of which is shaped by phenomena such as active galactic nuclei (AGN) winds and supernova explosions [6].

Among the most potent tools for probing the elusive baryon distribution is the measurement of the Sunyaev-Zel'dovich (SZ) effect around galaxies. Stemming from the interaction of free electrons in the CGM and ICM with cosmic microwave background (CMB) photons, the SZ effect provides a window into the thermodynamic properties of galaxy groups and clusters, critical for resolving a multitude of astrophysical and cosmological enigmas. In particular, the thermal Sunyaev-Zel'dovich (tSZ) effect arises from the inverse Compton scattering of CMB photons by the hot thermal gas within groups and clusters. Its magnitude, directly proportional to the electron pressure integrated along the line-of-sight, offers insights into the thermodynamic conditions of these cosmic structures. In contrast, the kinematic Sunyaev-Zel'dovich (kSZ) effect results from the encounters between CMB photons and free electrons in bulk motion relative to the CMB rest-frame. This effect depends on the integrated electron density along the line-of-sight, multiplied by the peculiar velocity making it a powerful tool for tracing the spatial distribution of baryons, even to the outskirts of galaxies and clusters (e.g., see [7, 8] for a review on the SZ effect). In particular, the kSZ effect can be used to measure the gas density in the outskirts of galaxies, independent of any assumptions on temperature or metallicity.

In this work, we measure the baryon profiles around Dark Energy Spectroscopic Instrument (DESI) luminous red galaxies (LRGs) using the stacking of the kSZ effect, which has been measured using a variety of techniques over the years [9–13]. Our findings shed light on the complex relationship between baryonic matter and dark matter. The novelty of this work lies in the following three aspects: 1) its pioneering use of photometric redshifts for probing the stacked kSZ effect, which departs from the traditional use of spectroscopic redshifts; 2) challenging the predictions of state-of-the-art hydrodynamical simulations – we find that the feedback processes appear to be stronger in the real Universe than in simulations – in other words, the baryons are expelled more violently from the cores of galaxy groups and clusters; 3) its implications for alleviating or resolving discrepancies in weak lensing analysis; most notably, the 'low S_8' tension found when comparing the inferred values of the clumpiness parameter, $S_8 \equiv \sigma_8(\Omega_m/0.3)^{1/2}$, from weak lensing with CMB probes (e.g., see [14] and references therein), and the 'Lensing is low' tension, which constitutes a discrepancy between galaxy clustering and galaxy-galaxy lensing [15, 16].

This paper is organized as follows. Section II and Section III offer a description of our data and methodology, respectively, while Section IV describes our results. Section V discusses the broader implications of our findings for both astrophysics and cosmology, particularly their potential for addressing the S_8 and the 'Lensing is low' discrepancies.

II. DATA

A. DESI imaging survey

The Dark Energy Spectroscopic Instrument is a robotic, fiber-fed, highly multiplexed spectroscopic surveyor that operates on the Mayall 4-meter telescope at Kitt Peak National Observatory [17]. DESI, which can obtain simultaneous spectra of almost 5000 objects over a $\sim 3°$ field [18–20], is currently conducting a five-year dark energy survey of about a third of the sky [21]. This campaign will obtain spectra for approximately 40 million galaxies and quasars [22].

In this paper, we use the photometric sample of DESI Luminous Red Galaxies (LRGs) and a higher-density extended LRG sample, referred to as 'Main LRGs' and 'Extended LRGs' [23–27]. The parent imaging is the DESI Legacy Imaging Survey, which is a combination of optical and mid-infrared imaging used for DESI target selection from three telescopes: Blanco for Dark Energy Camera Legacy Survey (DECaLS), Mayall for the Mayall z-band Legacy Survey (MzLS), and Bok for the Beijing–Arizona Sky Survey (BASS). We also make use of the reliable photometric redshifts presented in Zhou *et al.* [27] for Data Release 9 (DR9) and Data Release 10 (DR10), which have been calibrated via DESI spectroscopic redshifts and thus have only a small fraction of contaminants and a mean error of $\sigma_z/(1+z) \lesssim 0.02$. Similarly to Zhou *et al.* [27], we define four tomographic bins: [0.4, 0.54], [0.54 0.713], [0.713, 0.86] and [0.86 1.024] (see Table I for mean bin redshifts and number of galaxies in the overlap with ACT). We take into account the estimated error in the photometric redshifts for each galaxy, by imposing a maximum cut on the estimated error of $\sigma(z) < 0.05$. This removes $\sim$3% of the galaxies, including outliers with anomalously large redshift errors that could otherwise bias the reconstructed velocities by diluting the density signal [see 28, for tests on simulations]. In App. B, we investigate the effects of not imposing such a cut and find that, for the most part, they are negligible.

B. ACT temperature maps

This paper employs the harmonic-space Internal Linear Combination (hILC) maps [29, 30] from the Data Release 6 (DR6) from the Atacama Cosmology Telescope (ACT), a 6 m telescope that was located in the Atacama Desert of Chile and measured the CMB from 2007 to 2022. The DR6 data comprise multifrequency observations from 2017 to 2022 and the hILC map covers roughly a third of the sky (32%) at three frequency bands: f090 (77–112 GHz), f150 (124–172 GHz), and f220 (182–277 GHz), and uses *Planck* data on large scales [31, 32]. The observational program of DR6 targeted the 'wide' field. For this work, we use only the night-time portion of the data taken in the first five observing seasons (2017-2021). The ACT maps are produced in the plate-carrée (CAR) projection scheme. This analysis uses the first version of the ACT DR6 maps, dr6.01. Similarly to [33], we apply a mask on the ACT map that removes all detected clusters [34] and point sources as well as 5σ outliers in any of the filtered temperature bins, since those can bias the stacked profiles.

III. METHODS

A. Reconstruction

If we naively stacked the kSZ signal around a sample of galaxies, the effect would cancel out, as each object has an equal chance of moving towards or away from the observer. Therefore, to selectively extract the kSZ effect from CMB maps, we employ an estimate of the peculiar velocity of each galaxy in the line-of-sight direction, reconstructed from the three-dimensional galaxy overdensity field. In particular, we can obtain an estimate of the line-of-sight velocity field by solving the linearized continuity equation in redshift space [35], similarly to the reconstruction method applied in Baryon Acoustic Oscillations (BAO) analysis:

$$\nabla \cdot \boldsymbol{v} + \frac{f}{b} \nabla \cdot [(\boldsymbol{v} \cdot \hat{\boldsymbol{n}})\hat{\boldsymbol{n}}] = -aHf\frac{\delta_g}{b}, \tag{1}$$

where δ_g is the observed galaxy overdensity field, $\boldsymbol{v}$ is the peculiar velocity field, $\hat{\boldsymbol{n}}$ is the line-of-sight unit vector, $H(z)$ is the redshift-dependent Hubble parameter, f is the logarithmic growth rate, defined as $f \equiv d\ln(D)/d\ln(a)$ with $D(a)$ the growth factor and a the scale factor. Here, we assume that the galaxy overdensity δ_g is related to the matter overdensity, δ, by a linear bias factor, b, such that $\delta_g = b\delta$.

We construct the galaxy overdensity field separately in each tomographic bin. Due to the difference in the depth of the three regions that make up our sample, designated 'DES', 'N' and 'S', we generate the sample of randoms for each region before joining them back together to evaluate the galaxy overdensity field in the given tomographic bin.

In order to obtain an estimate of the peculiar velocity of each galaxy, we adopt the standard BAO reconstruction method of [36], implemented in the package `pyrecon` [1] [37]. This method yields an estimate of the first-order galaxy displacement field, which can be converted into an estimate for the velocity. A study performed on realistic DESI-like light cone mocks [28] informs us that the cross-correlation coefficient, $r \equiv \langle v_{||}^{\rm halo} v_{||}^{\rm rec}\rangle / \sigma_{||}^{\rm halo}\sigma_{||}^{\rm rec}$, between the reconstructed galaxy velocities along the line-of-sight (denoted by subscript $||$) and the host halo velocities, which captures imperfections in the velocity reconstruction, is about $r \approx 0.3$ (with an uncertainty of about 10%), the value we adopt in this study, while that of the spectroscopic sample is about $r \approx 0.64$. In other words, the reconstruction performance deteriorates by about half when using photometric redshifts, a prediction also confirmed by a similar study in the 'snapshot geometry' [38]. Nonetheless, the measurement around the photometric LRG sample yields a high signal-to-noise ratio (SNR) due to the large number of galaxies comprising the imaging survey. We note that LRGs are found mostly in galaxy groups with a mean linear bias of $b \approx 2.2$ [39]. In addition to the cuts in [33], for our fiducial analysis, we remove outliers in the reconstructed velocities and CAP-filtered temperature at the largest apertures measured (6 arcmin) at 3σ [2] and ensure that the number of galaxies in each velocity bin is symmetric around the mean by random down-sampling, which avoids unwanted biases from massive clusters and guarantees that in the absence of a kSZ signal, our estimator yields zero mean signal. In App. B, we show that these corrections have a mostly negligible effect: the uncorrected measurements tend to have marginally higher SNR (as a result of the larger number of galaxies in the samples) except for bin 3, which has a lower SNR due to its slightly asymmetric line-of-sight velocity distribution that improves once we remove the outliers.

B. Estimator

Once we have estimates of the velocities, we can measure the CMB temperatures $\mathcal{T}_i(\theta_d)$ around each galaxy i using a compensated aperture photometry (CAP) filter [33]. There are several benefits to using the CAP filter. Unlike a matched filter, the CAP filter is agnostic about the profile shape and because it is measured at different radii, it allows us to reconstruct the spherically averaged profiles. It is very effective at removing the large-scale primary CMB, as well as the uncorrelated part of the signal, leaving, in principle, only the sum of the one- and two-halo terms [see 40, for tests on simulations]. Additionally, the CAP-filtered profiles behave similarly to a cumulative density profile for large radii. The CAP filter is defined as:

$$\mathcal{T}(\theta_d) = \int \mathrm{d}^2\theta \, \delta T(\theta) \, W_{\theta_d}(\theta) \, . \tag{2}$$

where $\delta T(\theta)$ are the CMB temperature fluctuations and the filter W_{θ_d} is chosen as:

$$W_{\theta_d}(\theta) = \begin{cases} 1 & \text{for}\, \theta < \theta_d \, , \\ -1 & \text{for}\, \theta_d \le \theta \le \sqrt{2}\theta_d \, , \\ 0 & \text{otherwise.} \end{cases} \tag{3}$$

[1] `https://github.com/cosmodesi/pyrecon`

[2] Objects that are simultaneous outliers in both temperature and reconstructed velocity at 3σ constitute $\lesssim$0.1%.

LRG sample	# of galaxies	$z_{\rm mean}$	$\chi^2_{\rm null}$	$\mathrm{SNR}_{\rm DM}$	$\mathrm{SNR}_{\rm null}$
Ext. DR9 $z_{\rm bin=1}$	963,631	0.47	43.2	19.9	6.4
Ext. DR9 $z_{\rm bin=2}$	1,658,313	0.63	69.4	21.6	7.1
Ext. DR10 $z_{\rm bin=3}$	1,951,646	0.79	80.3	26.1	8.2
Ext. DR10 $z_{\rm bin=4}$	1,690,171	0.92	34.0	14.6	4.6
Ext. DR9+10 all	6,850,072	0.75	203.0	42.9	13.5
Main DR9 $z_{\rm bin=1}$	422,350	0.47	25.2	13.7	4.4
Main DR9 $z_{\rm bin=2}$	795,393	0.63	78.8	24.4	7.8
Main DR10 $z_{\rm bin=3}$	753,945	0.79	65.9	23.4	7.3
Main DR10 $z_{\rm bin=4}$	629,367	0.93	20.8	10.1	3.2
Main DR9+10 all	2,882,904	0.74	166.7	38.8	12.1

TABLE I. Statistics of the detection for each redshift bin and LRG sample in terms of the null $\chi^2_{\rm null}$, the SNR with respect to null, defined as $\mathrm{SNR}_{\rm null} \equiv (\chi^2_{\rm null} - \chi^2_{\rm bf})^{\frac{1}{2}}$, with best-fit coming from the Illustris-1 simulation curves at $z = 0.5$ (see Fig. 2), and SNR with respect to the dark matter distribution (empirical from gravity-only simulations), defined as $\mathrm{SNR}_{\rm DM} \equiv (\chi^2_{\rm DM} - \chi^2_{\rm bf})^{\frac{1}{2}}$. Results are shown for the DR10 LRGs; see Table III for DR9. We detect the signal at 13.5σ and 12.1σ for the Extended and Main sample, respectively, and at 42.9σ and 38.8σ with respect to a dark-matter-only profile.

Thus, we add the integrated temperature fluctuation in a disk with radius θ_d and subtract a concentric ring of the same area as the disk, at each radial bin. Similarly to [33], we choose nine radial bins, θ_d, spanning between 1 and 6 arcmin. For the four redshift bins (see Table I), this range corresponds roughly to a physical range of (0.36, 2.2), (0.42, 2.5), (0.46, 2.8) and (0.48, 2.9) Mpc, respectively.

We adopt the velocity-weighted, uniform-mean estimator from [33]:

$$\hat{T}_{\rm kSZ}(\theta_d) = -\frac{1}{r}\frac{v^{\rm rec}_{\rm rms}}{c}\frac{\sum_i \mathcal{T}_i(\theta_d)(v_{{\rm rec},i}/c)}{\sum_i (v_{{\rm rec},i}/c)^2}, \quad (4)$$

where $v^{\rm rec}_{\rm rms}$ is the rms of the radial component of the reconstructed velocities, $v_{{\rm rec},i}$, c is the speed of light, and r is the cross-correlation coefficient between the reconstructed and true velocity, evaluated from mock simulations. We use the publicly available pipeline `ThumbStack`[3] to apply the estimator to the DESI and ACT data.

To interpret the kSZ profiles obtained through the above method, we need to estimate the covariance of the stacked measurements. We do so by applying a bootstrap resampling to the signal at each galaxy location. In particular, we draw 10,000 realizations of the galaxy catalogs (with repetition), and infer the covariance matrices from the scatter across the resampled stacked profiles (see Section IV E).

[3] `https://github.com/EmmanuelSchaan/ThumbStack`

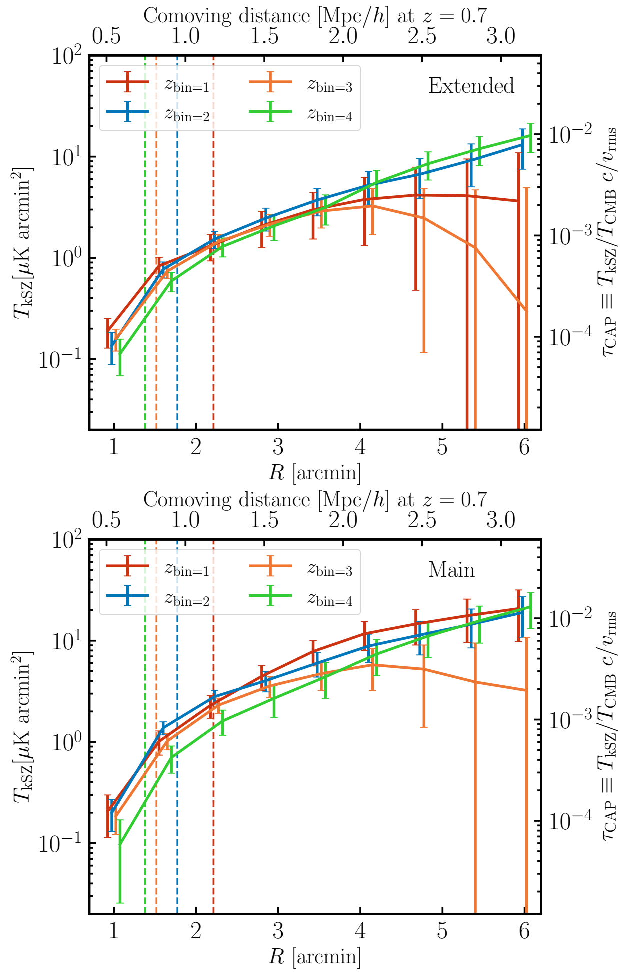

FIG. 1. Stacked kSZ signal in each redshift bin of the photometric LRG sample (*top:* Extended, *bottom:* Main) as a function of radius of the CAP filter, which approximately corresponds to the distance from the galaxy group center associated with the LRGs. The kSZ signal is obtained by stacking the hILC ACT DR6 map (with an effective FWHM = 1.6′) and is detected at $> 10\sigma$ relative to dark matter in each bin (see Table I). The vertical dashed line indicates the mean virial radius of the host halos for each bin. We show the full covariance of the data in App. IV E and note that the points at large aperture are significantly correlated. We see that the gas profile is well extended beyond the virial radius, suggesting that the feedback activity in LRG halos is strong enough to push much of the gas away from the galaxy group center. The top x axis and the right y axis show the comoving distance and $\tau_{\rm CAP}$ at the mean redshift.

IV. RESULTS

A. Stacked kSZ signal per redshift bin

Fig. 1 shows the stacked kSZ signal (Eq. 4) from ACT for the four photometric bins of the DR10 Extended and Main LRG samples obtained from the DESI Imaging Survey (see Section II A). The signal is shown as a function of CAP filter radius and detected at a high significance. We note that the error bars at large aperture are highly correlated (see Fig. 5). To aid interpretation, we convert the x and y axis into proper distance and CAP-filtered optical depth ($\tau_{\rm CAP} = T_{\rm kSZ}/T_{\rm CMB}\ c/v_{\rm rms}$), respectively, calculated at the mean redshift, $z \approx 0.7$. We note that the optical depth measures the integrated gas density along the line-of-sight,

$$\tau(z) \equiv \int n_e(\chi\hat{\boldsymbol{n}}, z)\sigma_T \frac{{\rm d}\chi}{1+z}, \quad (5)$$

where σ_T is the Thomson scattering cross section, χ is the comoving distance to redshift z, and n_e is the free electron physical number density.

In Table I, we show the significance of detection and corresponding SNR and chi-squared values for each of the four bins as well as the combination of all four bins. We define the SNR with respect to null[4] as $\mathrm{SNR}_{\rm null} \equiv (\chi^2_{\rm null} - \chi^2_{\rm bf})^{\frac{1}{2}}$, with best-fit coming from the Illustris-1 simulation[5] curve at $z = 0.5$ (see Fig. 2 for more details) with a freed up parameter for the amplitude, and the SNR with respect to the dark matter distribution (with amplitude fixed by the theory best fit), defined as $\mathrm{SNR}_{\rm DM} \equiv (\chi^2_{\rm DM} - \chi^2_{\rm bf})^{\frac{1}{2}}$. We detect the signal at $\sim 13\sigma$ and find the profiles to differ from the dark matter ones by $\sim 40\sigma$. The dark matter profiles are obtained by stacking on dark-matter-only maps computed using the TNG300-1-Dark simulation (dark-matter-only counterpart to TNG300-1), and we have tested that other dark-matter-only simulations (e.g., Illustris-1-Dark) yield fully consistent results, as expected for pure N-body simulations. The χ^2 metric is defined in the standard way using the covariance matrix C from Fig. 5:

$$\chi^2_{\rm model} \equiv (D - M)^T C^{-1} (D - M)\ , \quad (6)$$

where D is our stacked kSZ measurementfrom the data, and M is the model we are comparing against (if null, $M = 0$).

To take advantage of the larger number of objects in DR9 and their relatively smaller photometric z errors at low z (compared with high z), we quote the DR9 results for bin 1 and 2 and the DR10 results for bin 3 and 4. For the combined 'DR9+10 all,' we use DR10 reconstructed velocities where available and otherwise DR9 ones in order to maximize the signal. We provide detailed comparison between DR9 and DR10 in Tables II and III finding a high level of congruence between the two. Compared with the previous measurement using CMASS LRGs and ACT DR4 [33], $\chi^2_{\rm null} \approx 86$ (same number of radial bins), we see that the total chi-squared for our Extended and Main samples is $\chi^2_{\rm null} \approx 200$ and 170, respectively, or about twice higher. In App. A, we find our curves to be in excellent agreement with [33].

Intuitively, one can think of these curves as showing roughly the cumulative gas density distribution. At large radii, we expect the profiles to become shallower as more and more of the gas is enclosed. We see that the gas profiles are steep beyond the virial radius, suggesting that a significant fraction of the gas resides beyond it (see discussion of Fig. 2, where we test this conjecture). The decline in amplitude at large apertures of bin 3 is due to noise from the primary CMB and the larger fraction of photometric z outliers in that bin (see App. B).

[4] Corresponding to the inverse of the fractional error on the fit of a single amplitude parameter to the data. This often called the "detection significance" in number of Gaussian standard deviations σ.

[5] https://www.tng-project.org/data/

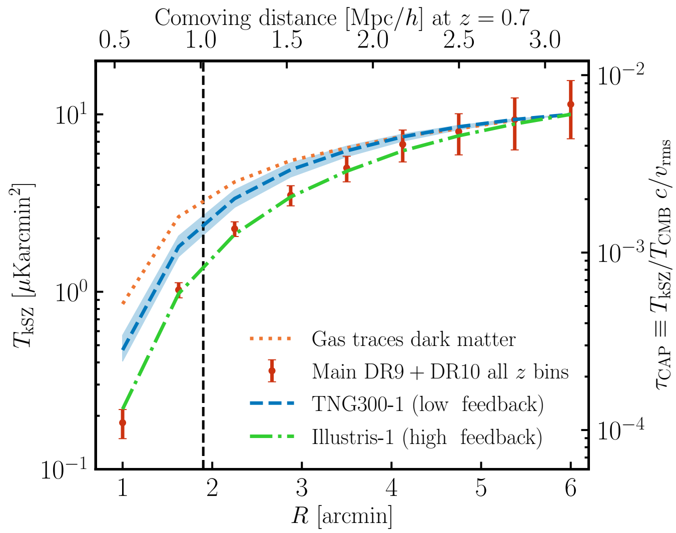

FIG. 2. Comparison between the kSZ signal from the combined Main sample from all redshift bins (red error bars) and the modeled kSZ signal from the TNG and Illustris simulations. These curves approximate the cumulative gas profiles at large radii. The right y axis converts the kSZ signal into a measure of the optical depth τ, i.e., the integrated gas density along the line-of-sight, via $\tau = T_{\rm kSZ}/T_{\rm CMB} c/v_{\rm rms}$. The top x axis shows the gas profiles as a function of comoving distance from the center of DESI groups. We find at a significance of 40σ that the gas is much more extended than the dark matter (red dotted curve). The large gap between the data and the TNG curve (blue dashed curve) indicates that the data disfavor strongly prescriptions of weak baryonic feedback in simulations. In contrast with TNG, the old Illustris model (green dash-dotted curve) appears much more consistent with the data, implying that models with large baryonic feedback are preferred. The simulation curves are multiplied by $O(1)$ to match the data at high radius factor for visual purposes (see the text). The vertical line shows the mean virial radius for this sample. The thin blue band around the TNG curve represents the range of alternative scenarios considered (see the text). We show the full covariance of the data in App. IV E.

B. Comparison with simulations

In Fig. 2, we study the comparison between the state-of-the-art hydrodynamical simulations IllustrisTNG-300-1 (TNG300-1) [41] and the measured gas profiles from the data. We also show a comparison with the older model of the Illustris-1 simulation [42], which has known shortcomings with predicting observations such as galaxy morphologies and colors, various cluster properties, and gas fractions [41, 43, 44]. We select LRG-like galaxies in the two simulations via an abundance matching approach and stack them at their locations on 2D CMB data mimicking ACT maps[6]. Namely, we rank-order the galaxies by stellar mass and select the top $N_{\rm gal}$ such that, $N_{\rm gal}/L^3 \sim 5.4\times10^{-4}$ $[{\rm Mpc}/h]^{-3}$ for the Main sample and 1.2×10^{-3} $[{\rm Mpc}/h]^{-3}$ for the Extended sample. We find that the mean halo mass of LRGs in TNG300-1 matches very well the inferred mean halo mass of DESI LRGs at $0.4 < z < 0.6$, $10^{13.4}$ $M_\odot/h$, and at $0.6 < z < 0.8$, $10^{13.2}$ $M_\odot/h$ [39]. In Section IV D, we split the galaxies into stellar mass bins estimated in [26] and detect the mass evolution of the signal at high significance.

Of most interest in this study is comparing the shapes of the profiles rather than the overall normalization, as the shapes encode information about the extent of the gas and hence the strength of the baryonic feedback effects. To make the comparison more straightforward, we multiply the TNG300-1 and Illustris-1 curves by a $\mathcal{O}(1)$ factor to match the amplitude of the data at the penultimate CAP radial bin. We find that there is a noticeable gap between the TNG300-1 prediction and the observed profiles, whereas the Illustris-1 model appears to be in much better agreement with the data. This result suggests stronger feedback is needed than present in TNG300-1, of similar magnitude to the older Illustris-1 model, which is known to have strong baryonic feedback. This result also suggests that the 'S_8 tension' in weak lensing [14] could be partially explained by baryonic effects (see also Ref. [45]), and we leave a more detailed study for future work.

We perform a number of tests on both hydrodynamical simulations to ensure that the gap we see is significant: we vary the satellite fraction from 0% to 30%[7] (note that the constraints from [39] are 11 ± 1%), we put all galaxies at the centers of their host halos, we vary the number density (between half and twice the fiducial value, i.e. from 3×10^{-4} to 1×10^{-3} $[{\rm Mpc}/h]^{-3}$) and thus stellar mass threshold of the extracted LRGs, and we add noise to the halo velocities. In Fig. 2, we show the default scenario for both simulations and in shaded color for TNG300-1, we display the minimum and maximum deviations from the default caused by all the aforementioned alternative scenarios. Despite considering scenarios that push the bounds of physically reasonable models, we see that the gap between simulations and observations persists. In fact, we find a significant deviation of 17σ (19σ) between the kSZ signal of the combined Main (Extended) sample and that of TNG300-1, defined as ${\rm SNR}_{\rm TNG300\text{-}1} \equiv (\chi^2_{\rm TNG300\text{-}1} - \chi^2_{\rm bf})^{\frac{1}{2}}$ where once again we adopt the Illustris curve at $z = 0.5$ as our theory curve with a free amplitude that is then used to rescale the TNG300-1 curve by. We stress that in quoting these numbers we fully marginalize over the amplitude of the signal. Future simulation efforts would need to focus on reconciling their outputs with our observed gas profiles from kSZ.

[6] Prior to applying any filter, these maps are convolved with the ACT beam, in this case a Gaussian with FWHM = 1.6 arcmin before being passed to the stacking pipeline.

[7] Centrals are selected as the most massive subhalo in each host halo. To vary the satellite fraction, we randomly discard centrals or satellites.

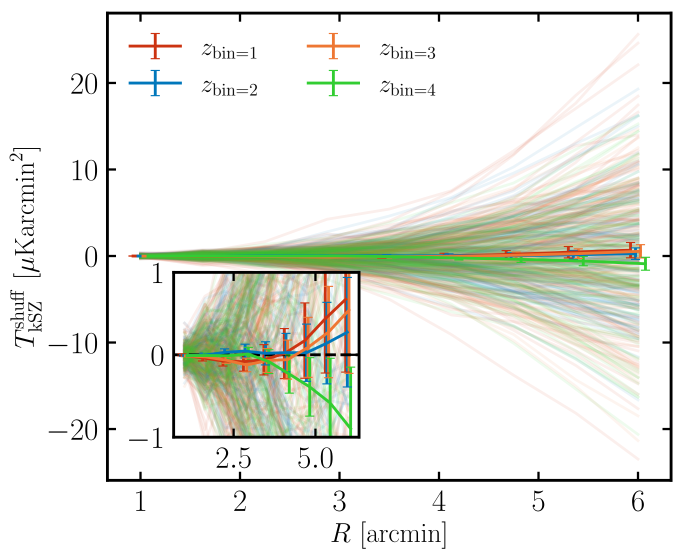

FIG. 3. Null test demonstrating that there are no substantial systematics affecting our measurement such as residual CIB or tSZ contamination. The result is obtained by randomly shuffling the reconstructed velocities at the location of each DESI LRG before performing the stacking of the signal. The set of 1000 random reshuffles is shown as faint lines with its mean and error on the mean as solid lines. Reassuringly, it is consistent with zero and the largest deviations, $\sim$1, are much smaller ($\sim$10 times) than the size of the signal (Fig. 1).

C. Null test

In Fig. 3, we validate that our measured signal is indeed due to the kSZ effect rather than correlated contaminants such as the cosmic infrared background (CIB) or tSZ. For this test, we shuffle randomly the sample of reconstructed velocities to obtain 1000 realizations and perform the stacking of Eq. 4 but using the shuffled velocities on each galaxy. Since the true kSZ effect is proportional to the line-of-sight velocity, deleting that information in the shuffling should lead to a null measurement, which is indeed what we find. The tSZ and CIB effects do not have such dependence[8], and hence if our ACT map is correctly cleaned, any additive contamination should also vanish. We note that this argument also holds true for the unshuffled (original) kSZ measurement, which is robust to additive contributions.

D. Mass evolution

Understanding the mass evolution of baryonic feedback is key to properly modeling its effect on cosmological observables such as cosmic shear, and the SZ effect is a versatile probe capable of capturing multiple gas properties

[8] Foreground emission such as from the CIB is also Doppler-boosted and acquires a term proportional to velocity. However, we find that this contribution is about two orders of magnitude smaller than the kSZ signal [46], and we'll therefore neglect it in this analysis.

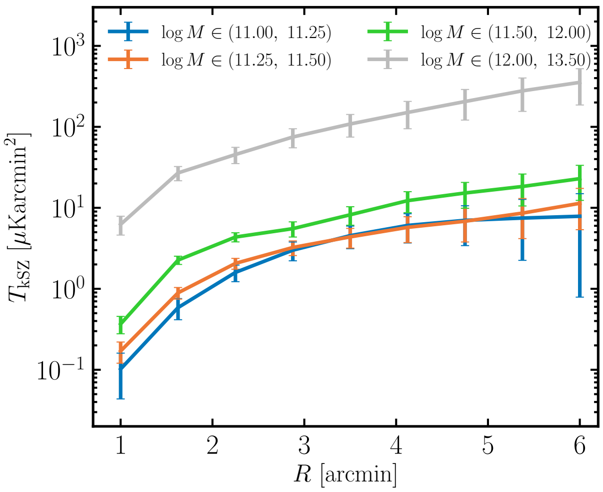

FIG. 4. As Fig. 2, but we show the kSZ stacked measurements for the combined (DR9+DR10) Main sample, split into stellar mass bins. We see a noticeable increase in the amplitude of the signal with mass and note that the relative differences between these amplitudes are immune to miscalibration of e.g., the cross-correlation coefficient r, and the rms of the velocity. As expected, the curves become shallower at small apertures, as the average host halo mass increases.

[see e.g., 47–52, for novel probes and methods]. Here we use estimates of the stellar mass from Zhou *et al.* [26] to split the galaxies in the combined (DR9+DR10) Main sample into four mass/luminosity bins: $\log M \in (11, 11.25), (11.25, 11.5), (11.5, 12)$, and $(12, 13.5)$, each containing 926,232, 1,362,717, 458,886, and 2,152 galaxies, respectively. We note that the estimated masses have not been thoroughly characterized, and thus, they are mostly used to make qualitative statements.

We show the kSZ stacked measurements for each bin in Fig. 4. We detect the individual signals at high significance. The null χ^2 is $\chi^2_{\rm null}$ = 29.7, 68.2, 96.2, and 28.3, and the deviation from the dark-matter profiles is SNR = 15, 24, 27, and 15σ, for each bin, respectively. As can be seen in the figure, we find a strong signature of the evolution of the amplitude with mass: namely, it increases with stellar mass/luminosity, as the optical depth is proportional to the total mass of the halo, i.e., the amplitudes of the stellar-mass bin samples differ roughly by the ratios of their respective mean stellar masses, since $\tau \propto M_{\rm halo} \propto M_*$. We note that the relative differences between the amplitudes are independent of the calibration of the cross-correlation coefficient r and the rms of the velocity. In addition, as expected, the curves become shallower at small apertures, as the mass increases. This is the case because massive halos retain more gas within the virial radius, as they have deeper potential wells compared with their less massive counterparts. At large apertures, the points are extremely strongly correlated, and it is imprudent to draw any definite conclusions on this issue (see Fig. IV E). We leave a detailed analysis of the effect of baryons on weak lensing probes, as measured in this paper, for future work.

E. Covariance matrix

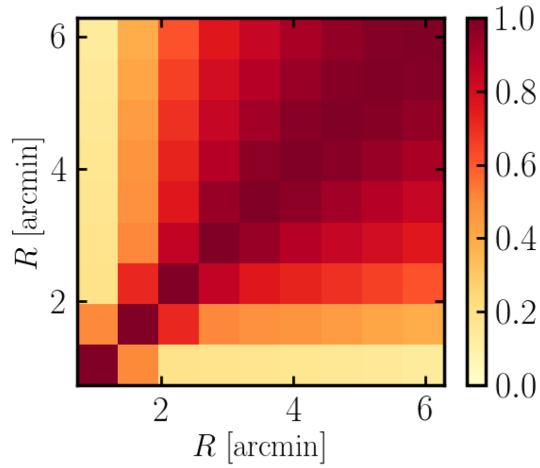

FIG. 5. Correlation matrix of the kSZ signal between the different CAP filter radii for the first photometric bin. The correlation between different CAP radii is stronger on large scales, as the fluctuations of the primary CMB become dominant on these scales. We note that the structure of the correlation function is the same for all samples.

The covariance matrix of the data is obtained by drawing 10,000 realizations of the galaxy catalogs (with repetition) and computing the covariance matrices from the resampled stacked profiles, i.e. bootstrapping. This produces an unbiased estimate of the covariance, in the limit of independent noise realizations from galaxy to galaxy. The assumption is not correct for large apertures where the temperature map cutouts (submaps) overlap, and the inferred covariance is only accurate at the 10% level (see [33]). However, given our errorbars, this level of accuracy is sufficient.

The covariance matrix for the first photometric bin is shown in Fig. 5. On small scales, the covariance is dominated by the detector noise in the temperature maps. Because this noise is mostly white and uncorrelated across frequencies, the small-aperture measurements are mostly uncorrelated within each submap and across submaps. On large scales, the covariance receives a large contribution from the primordial CMB fluctuations, which are shared between the aperture measurements in each submap and across submaps (and different CMB frequency maps). Due to this effect, which leads to diminishing returns in the SNR at larger apertures, the maximum aperture we consider is 6 arcmin.

In Fig. 6, we illustrate the stacked 2D kSZ signal for the Main DR9 sample of DESI LRGs. We apply a Wiener filter ($C_\ell^{\rm kSZ}/C_\ell^{\rm tot}$) that effectively high-pass filters the CMB temperature map to isolate the small-scale signal that is the most affected by the kSZ effect. We can see by eye the extended gas envelope of the DESI LRGs, which spans several arcmin. This roughly corresponds to the mean halo virial radius at that redshift.

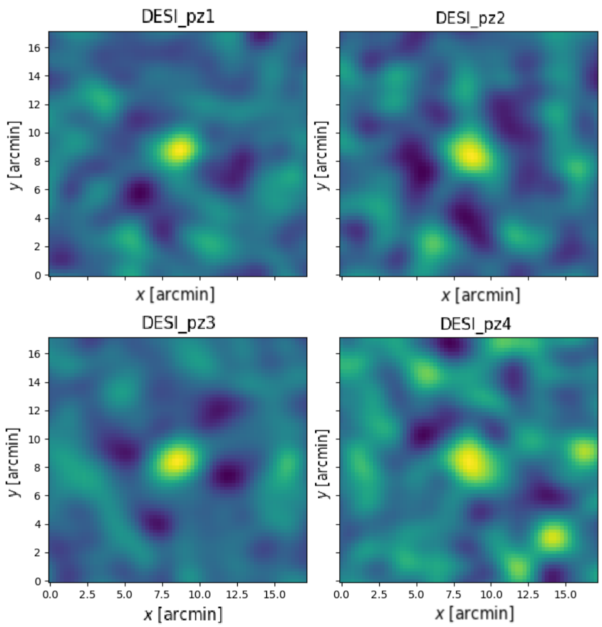

FIG. 6. 2D maps of the stacked kSZ signal around DESI DR9 LRGs in the Main sample for all four photometric bins. For visual purposes only, we high-pass filter the CMB temperature map before performing the stacking, as the fluctuations of the primary CMB are dominant in the ∼10 arcmin regime. Thus, we can clearly see the gas envelope of the DESI LRGs, which as expected, extends for several arcmin, i.e., is of the same order of magnitude as the mean halo virial radius at that redshift.

V. SUMMARY AND IMPLICATIONS

In this paper, we present the highest SNR measurement of the gas profiles around galaxy groups using the kSZ effect: we detect the signal at 13σ and find that it deviates from the dark matter at 40σ (see Fig. 1 and Table I). Such strong baryonic feedback exceeds predictions from state-of-the-art hydrodynamical simulations such as IllustrisTNG (TNG300-1). It also suggests that baryons might play a more significant role than assumed in many cosmological analyses and alleviate tensions such as 'Lensing is low' and 'Low S_8.' Properly accounting for baryonic feedback is critical to placing robust constraints on many open questions, including the mass of neutrinos and the nature of dark matter – questions that will be crucial to future cosmological surveys such as *Roman*, *Euclid*, and the Vera Rubin Observatory. Our measurements of the gas profiles can be used to calibrate the subgrid models of hydrodynamical simulations, a task typically complicated by the low detection sensitivity to gas on the outskirts of halos (i.e., the 'missing baryon' problem). Combining kSZ measurements with tSZ and X-ray measurements, which provide access to additional quantities such as the temperature and cooling rate around galaxies [53, 54], will enable us to fully solve the gas thermodynamics of groups and clusters and shed light on the role of feedback in galaxy evolution.

To put our findings into perspective in relation to the S_8 tension, we offer a back-of-the-envelope calculation. The value of the S_8 parameter as measured by cosmic shear surveys is about 10% lower than the *Planck* values [14], suggesting a ∼20% suppression to the matter power spectrum relative to a dark-matter-only universe across a range of scales $k = 0.1 \sim 10h/\mathrm{Mpc}$. Let's consider a point halfway between these values, at $k = 1h/\mathrm{Mpc}$. Assuming that the gas and dark matter follow a Gaussian profile [33], $k \sim 1h/\mathrm{Mpc}$ corresponds to $R \sim 1\mathrm{Mpc}/h$. As seen from Fig. 2, at $R \sim 1\mathrm{Mpc}/h$ about half of the gas is missing relative to the dark matter at a significance of $\sim 6\sigma$, which would manifest itself in the matter power spectrum as a 16% suppression with an uncertainty of ∼3% (assuming that baryons make up 16% of the total matter). This is roughly the effect of baryons needed to explain the S_8 tension, as suggested in Fig. 6 in Ref. [45] and Fig. 6 in Ref. [55], and ball-park matches the 20% suppression on the matter power corresponding to the measured S_8 value in cosmic shear experiments. Additionally, we note that our 13σ detection of the gas can be converted into a ∼2.5% modeling error on the matter power spectrum (assuming a single fitting parameter for the amplitude), which is well beyond the required accuracy for future experiments (e.g., the Vera Rubin Observatory). As such, weak lensing studies taking into account kSZ measurements to model the effect of baryons will be especially powerful for future cosmic shear analyses [56].

To make the kSZ measurement, we use the ACT temperature map and the DESI photometric galaxy sample of LRGs, which we split into four redshift bins. We detect the signal with respect to the dark matter in each of them at $\gtrsim 10\sigma$ (see Table I). This allows us to study for the first time the redshift evolution of the baryonic feedback through kSZ stacking and place tighter constraints on the allowed astrophysical feedback models. The fact that we see little evolution of the signal suggests that the population of red galaxies probed by DESI is fairly stable and that the AGN feedback is of similar magnitude across $z = 0.4 \sim 1$. A major advantage of the gas profiles obtained using the kSZ is that they are practically systematics-free, as the velocity-weighted stacking we perform cancels additive contaminants such as the tSZ and CIB (see Fig. 3 and Schaan *et al.* [12]). Importantly, unlike many other astrophysical probes, the signal is directly proportional to the amount of gas and independent of other properties such as temperature. To put our findings into perspective, we compare the observed gas density profiles with mock measurements extracted from the state-of-the-art hydrodynamical simulation TNG300-1 and its predecessor Illustris-1. In particular, we mimic the stacking and LRG selection process of the observational analysis and test various scenarios related to the simulation targeting choices (satellite fraction, number density, halo mass, velocity uncertainty) to quantify the allowed variations (see Fig. 2). We find that the baryonic feedback in the TNG300-1 simulation is not sufficiently strong to push enough of the gas out of the halo virial radius, whereas Illustris-1 accomplishes that more successfully. Future work examining the origin of this is instrumental to reconciling the theory and observations of the gas-dark matter link.

As the first study of the kSZ signal measured around a photometric sample of galaxies with reconstructed velocities, this work opens the door for an exciting new line of research with imaging surveys such as the large-scale projects Vera Rubin Observatory and *Euclid*, which will provide not only a much larger number of objects compared with their spectroscopic counterparts, but also more diverse samples that cover a wider range of redshifts, masses, morphologies, colors and environments. Understanding the connection between gas and dark matter will not only aid future cosmology analyses, but also help our understanding of galaxy formation and evolution. This paper adds an essential piece to a growing body of works aiming to unravel the complexities of cosmic gas in the era of large cosmological surveys.

ACKNOWLEDGMENTS

Data points for the figures are available at https://doi.org/10.5281/zenodo.12633573.

We would like to thank Minh Nguyen, Vid Irsic, Alex Amon, Daniel Gruen, and Yulin Gong for providing useful comments during the preparation of this manuscript.

B.H. thanks the Miller Institute for financially supporting her postdoctoral research. S.F. is supported by Lawrence Berkeley National Laboratory and the Director, Office of Science, Office of High Energy Physics of the U.S. Department of Energy under Contract No. DE-AC02-05CH11231. B.R. and E.S. received support from the U.S. Department of Energy under contract number DE-AC02-76SF00515 to SLAC National Accelerator Laboratory. This research used resources of the National Energy Research Scientific Computing Center (NERSC), a U.S. Department of Energy Office of Science User Facility located at Lawrence Berkeley National Laboratory, operated under Contract No. DE-AC02-05CH11231. The Flatiron Institute is supported by the Simons Foundation. EC acknowledges support from the European Research Council (ERC) under the European Union's Horizon 2020 research and innovation programme (Grant agreement No. 849169). MM acknowledges support from NSF grants AST-2307727 and AST-2153201 and NASA grant 21-ATP21-0145. GSF acknowledges support through the Isaac Newton Studentship and the Helen Stone Scholarship at the University of Cambridge. GSF and FQ furthermore acknowledge support from the European Research Council (ERC) under the European Union's Horizon 2020 research and innovation programme (Grant agreement No. 851274). CS acknowledges support from the Agencia Nacional de Investigación y Desarrollo (ANID) through Basal project FB210003. CS acknowledges support from the Agencia Nacional de Investigación y Desarrollo (ANID) through Basal project FB210003. RH acknowledges funding from the NSERC Discovery Grant RGPIN-2018-05750 and the Connaught Fund. This research was enabled in part by support provided by the SciNet cluster and the Digital Research Alliance of Canada. This work was supported by a grant from the Simons Foundation (CCA 918271, PBL).

This material is based upon work supported by the U.S. Department of Energy (DOE), Office of Science, Office of High-Energy Physics, under Contract No. DE–AC02–05CH11231, and by the National Energy Research Scientific Computing Center, a DOE Office of Science User Facility under the same contract. Additional support for DESI was provided by the U.S. National Science Foundation (NSF), Division of Astronomical Sciences under Contract No. AST-0950945 to the NSF's National Optical-Infrared Astronomy Research Laboratory; the Science and Technology Facilities Council of the United Kingdom; the Gordon and Betty Moore Foundation; the Heising-Simons Foundation; the French Alternative Energies and Atomic Energy Commission (CEA); the National Council of Humanities, Science and Technology of Mexico (CONAHCYT); the Ministry of Science, Innovation and Universities of Spain (MICIU/AEI/10.13039/501100011033), and by the DESI Member Institutions: https://www.desi.lbl.gov/collaborating-institutions. Any opinions, findings, and conclusions or recommendations expressed in this material are those of the author(s) and do not necessarily reflect the views of the U. S. National Science Foundation, the U. S. Department of Energy, or any of the listed funding agencies.

The authors are honored to be permitted to conduct scientific research on Iolkam Du'ag (Kitt Peak), a mountain with particular significance to the Tohono O'odham Nation.

The DESI Legacy Imaging Surveys consist of three individual and complementary projects: the Dark Energy Camera Legacy Survey (DECaLS), the Beijing-Arizona Sky Survey (BASS), and the Mayall z-band Legacy Survey (MzLS). DECaLS, BASS and MzLS together include data obtained, respectively, at the Blanco telescope, Cerro Tololo Inter-American Observatory, NSF's NOIRLab; the Bok telescope, Steward Observatory, University of Arizona; and the Mayall telescope, Kitt Peak National Observatory, NOIRLab. NOIRLab is operated by the Association of Universities for Research in Astronomy (AURA) under a cooperative agreement with the National Science Foundation. Pipeline processing and analyses of the data were supported by NOIRLab and the Lawrence Berkeley National Laboratory. Legacy Surveys also uses data products from the Near-Earth Object Wide-field Infrared Survey Explorer (NEOWISE), a project of the Jet Propulsion Laboratory/California Institute of Technology, funded by the National Aeronautics and Space Administration. Legacy Surveys was supported by: the Director, Office of Science, Office of High Energy Physics of the U.S. Department of Energy; the National Energy Research Scientific Computing Center, a DOE Office of Science User Facility; the U.S. National Science Foundation, Division of Astronomical Sciences; the National Astronomical Observatories of China, the Chinese Academy of Sciences and the Chinese National Natural Science Foundation. LBNL is managed by the Regents of the University of California under contract to the U.S. Department of Energy. The complete acknowledgments can be found at https://www.legacysurvey.org/.

Support for ACT was through the U.S. National Science Foundation through awards AST-0408698, AST-0965625, and AST-1440226 for the ACT project, as well as awards PHY-0355328, PHY-0855887 and PHY-1214379. Funding was also provided by Princeton University, the University of Pennsylvania, and a Canada Foundation for Innovation (CFI) award to UBC. ACT operated in the Parque Astronómico Atacama in northern Chile under the auspices of the Agencia Nacional de Investigación y Desarrollo (ANID). The development of multichroic detectors and lenses was supported by NASA grants NNX13AE56G and NNX14AB58G. Detector research at NIST was supported by the NIST Innovations in Measurement Science program. Computing for ACT was performed using the Princeton Research Computing resources at Princeton University, the National Energy Research Scientific Computing Center (NERSC), and the Niagara supercomputer at the SciNet HPC Consortium. SciNet is funded by the CFI under the auspices of Compute Canada, the Government of Ontario, the Ontario Research Fund–Research Excellence, and the University of Toronto. We thank the Republic of Chile for hosting ACT in the northern Atacama, and the local indigenous Licanantay communities whom we follow in observing and learning from the night sky.

Appendix A: Comparison with CMASS measurement

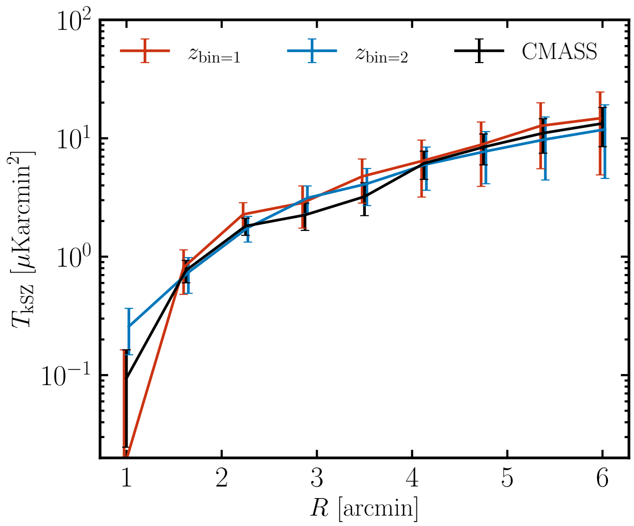

FIG. 7. Comparison between the DESI photo-z stacked kSZ signal in the first two redshift bins and the CMASS×ACT stacked kSZ measurement from [33]. Reassuringly, we see that the agreement with the first bin, which is closest in redshift to CMASS, $z_{\rm CMASS} \approx 0.55$ (cf. $z_{\rm bin=1} \approx 0.47$) is excellent. To make this visual comparison at the same frequency, we use the DR5 ACT maps at 90 GHz.

In Fig. 7, we show a comparison between the DESI photo-z stacked kSZ signal in each redshift bin and the old CMASS×ACT stacked kSZ measurement from [33]. We find excellent agreement between the two, in particular for the first redshift bin of our DESI result, which is closest in redshift to CMASS, $z_{\rm CMASS} \approx 0.55$ (cf. $z_{\rm bin=1} \approx 0.47$). We note that while the CMASS and the DESI LRG samples have similar host halo properties (e.g., mass, occupation distribution), they are not exactly the same, and therefore, this agreement should not be taken as a consistency check.

We emphasize that the combined chi-squared of all four bins, $\chi^2_{\rm null} \approx 200$, is about twice higher than that for CMASS×ACT, $\chi^2_{\rm null} \approx 86$. While the lower r value for our photometric sample reduces the SNR by about half, the improvement in number of objects (by 10-20 times depending on the sample), more than compensates for the loss.

Appendix B: Effect of removing corrections and comparison with Data Release 9

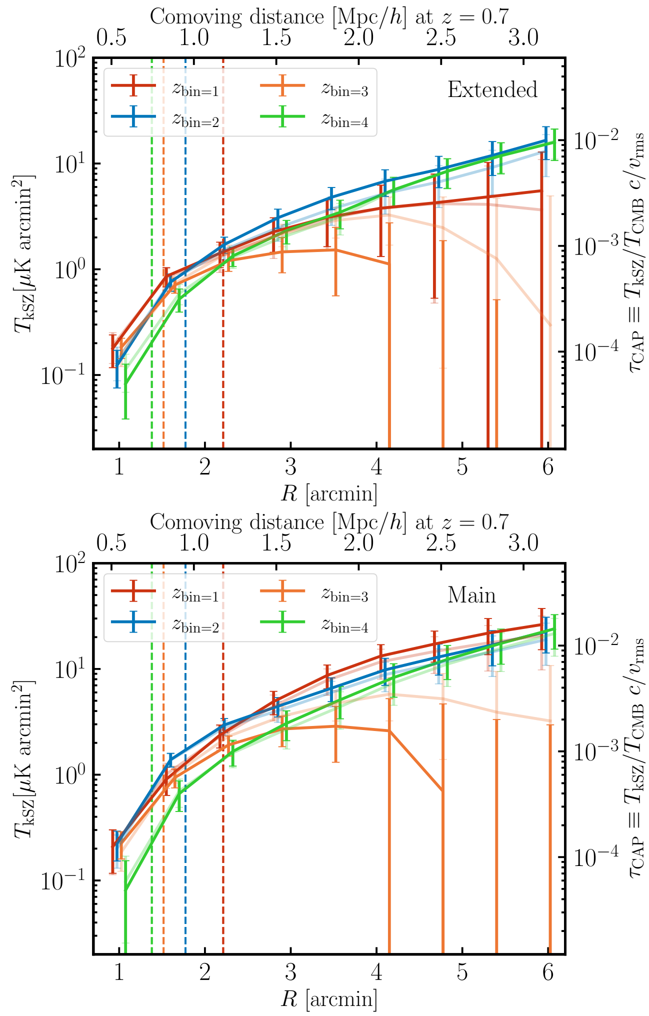

FIG. 8. Same as 1, but shown for the case where no corrections are applied. The fiducial measurement is shown as faded curves. We see that the two cases are in very good agreement.

As mentioned in the main text of this manuscipt, our fiducial measurement involves two additional cleaning techniques beyond the analysis of [33]: namely, removing photometric z outliers with estimated noise above $\sigma_z/(1+z) > 0.05$ and removing reconstructed velocity outliers at 3σ. In Table II, we compare the significance of the detection in the scenario of not applying each and any of these corrections.

Reassuringly, the three statistics of interest to this study, $\chi^2_{\rm null}$, $\rm SNR_{DM}$ and $\rm SNR_{null}$ are very similar in all four cases: both corrections (fiducial), only the photometric one, only the outlier one, and neither one applied. In particular, for the most part we see that the other three cases tend to have very similar if not slightly higher $\chi^2_{\rm null}$ compared with our fiducial analysis. We attribute this to the fact that the fiducial case features the smallest number of galaxies, having had a number of outliers removed.

A notable exception is the third photometric bin, which behaves better in the fiducial case than all others. Upon further inspection, we see that it has a slightly asymmetric reconstructed velocity distribution (possibly due to poorly reconstructed regions as a result of masking and/or photometric z miscalibration). Overall, the highest SNR is found in the case where only a photometric z error cleaning has been applied. We also note that the tails of the redshift distribution appear to be the largest in this bin [27].

To corroborate the claim that the additional cleaning applied in this work has minimal effect on the profile shapes, in Fig. 8, we present a comparison between the fiducial (cleaned) analysis and the case where neither of these corrections is applied. Visually, the curves bear a very strong resemblance with each other, all measurements being within 1σ of each other. Most prominently, we see that the third bin behaves more physically in the corrected case (since we adopt a CAP filter, we expect the measured profiles to increase until all gas is encompassed within some aperture radius), while the signal in the first bin gets a slight boost when no corrections are applied. This is reassuring to see, as it suggests that our cleaning procedure works as expected (i.e., it does not significantly bias our outputs and reduces the anomalous behavior exhibited by the third bin).

Furthermore, in Table III, we examine the stacked kSZ measurement coming from the DR9 samples and juxtapose it with the fiducial DR10 result. Overall, the DR10 signal is higher than the DR9 one. This is particularly true for the higher-redshift bins, for which the DR9 photometric redshift estimates are significantly worse than DR10 and a consequence of the fact that the i-band colors are very powerful at constraining higher redshift. Interestingly, we find a stronger detection for the first two bins due to the larger number objects in DR9 (not all galaxies have i-band colors measured). Similarly to the DR10 case, we find that often the uncorrected analysis yields a higher-significance detection but for the third bin. Once again the photo-z corrected sample boasts with some of the highest $\chi^2_{\rm null}$ values across all redshifts.

[1] M. Fukugita and P. J. E. Peebles, The Cosmic energy inventory, Astrophys. J. **616**, 643 (2004), arXiv:astro-ph/0406095.

[2] LSST Dark Energy Science Collaboration, Large Synoptic Survey Telescope: Dark Energy Science Collaboration, arXiv e-prints , arXiv:1211.0310 (2012), arXiv:1211.0310 [astro-ph.CO].

[3] Ž. Ivezić, S. M. Kahn, J. A. Tyson, B. Abel, E. Acosta, R. Allsman, D. Alonso, Y. AlSayyad, S. F. Anderson, J. Andrew, J. R. P. Angel, G. Z. Angeli, R. Ansari, P. Antilogus, C. Araujo, R. Armstrong, K. T. Arndt, P. Astier, É. Aubourg, N. Auza, T. S. Axelrod, D. J. Bard, J. D. Barr, A. Barrau, J. G. Bartlett, A. E. Bauer, B. J. Bauman, S. Baumont, E. Bechtol, K. Bechtol, A. C. Becker, J. Becla, C. Beldica, S. Bellavia, F. B. Bianco, R. Biswas, G. Blanc, J. Blazek, R. D. Blandford, J. S. Bloom, J. Bogart, T. W. Bond, M. T. Booth, A. W. Borgland, K. Borne, J. F. Bosch, D. Boutigny, C. A. Brackett, A. Bradshaw, W. N. Brandt, M. E. Brown, J. S. Bullock, P. Burchat, D. L. Burke, G. Cagnoli, D. Calabrese, S. Callahan, A. L. Callen, J. L. Carlin, E. L. Carlson, S. Chandrasekharan, G. Charles-Emerson, S. Chesley, E. C. Cheu, H.-F. Chiang, J. Chiang, C. Chirino, D. Chow, D. R. Ciardi, C. F. Claver, J. Cohen-Tanugi, J. J. Cockrum, R. Coles, A. J. Connolly, K. H. Cook, A. Cooray, K. R. Covey, C. Cribbs, W. Cui, R. Cutri, P. N. Daly, S. F. Daniel, F. Daruich, G. Daubard, G. Daues, W. Dawson, F. Delgado, A. Dellapenna, R. de Peyster, M. de Val-Borro, S. W. Digel, P. Doherty, R. Dubois, G. P. Dubois-Felsmann, J. Durech, F. Economou, T. Eifler, M. Eracleous, B. L. Emmons, A. Fausti Neto, H. Ferguson, E. Figueroa, M. Fisher-Levine, W. Focke, M. D. Foss, J. Frank, M. D. Freemon, E. Gangler, E. Gawiser, J. C. Geary, P. Gee, M. Geha, C. J. B. Gessner, R. R. Gibson, D. K. Gilmore, T. Glanzman, W. Glick, T. Goldina, D. A. Goldstein, I. Goodenow, M. L. Graham, W. J. Gressler, P. Gris, L. P. Guy, A. Guyonnet, G. Haller, R. Harris, P. A. Hascall, J. Haupt, F. Hernandez, S. Herrmann, E. Hileman, J. Hoblitt, J. A. Hodgson, C. Hogan, J. D. Howard, D. Huang, M. E. Huffer, P. Ingraham, W. R. Innes, S. H. Jacoby, B. Jain, F. Jammes, M. J. Jee, T. Jenness, G. Jernigan, D. Jevremović, K. Johns, A. S. Johnson, M. W. G. Johnson, R. L. Jones, C. Juramy-Gilles, M. Jurić, J. S. Kalirai, N. J. Kallivayalil, B. Kalmbach, J. P. Kantor, P. Karst, M. M. Kasliwal, H. Kelly, R. Kessler, V. Kinnison, D. Kirkby, L. Knox, I. V. Kotov, V. L. Krabbendam, K. S. Krughoff, P. Kubánek, J. Kuczewski, S. Kulkarni, J. Ku, N. R. Kurita, C. S. Lage, R. Lambert, T. Lange, J. B. Langton, L. Le Guillou, D. Levine, M. Liang, K.-T. Lim, C. J. Lintott, K. E. Long, M. Lopez, P. J. Lotz, R. H. Lupton, N. B. Lust, L. A. MacArthur, A. Mahabal, R. Mandelbaum, T. W. Markiewicz, D. S. Marsh, P. J. Marshall, S. Marshall, M. May, R. McKercher, M. McQueen, J. Meyers, M. Migliore, M. Miller, D. J. Mills, C. Miraval, J. Moeyens, F. E. Moolekamp, D. G. Monet, M. Moniez, S. Monkewitz, C. Montgomery, C. B. Morrison, F. Mueller, G. P. Muller, F. Muñoz Arancibia, D. R. Neill, S. P. Newbry, J.-Y. Nief, A. Nomerotski, M. Nordby, P. O'Connor, J. Oliver, S. S. Olivier, K. Olsen, W. O'Mullane, S. Ortiz, S. Osier, R. E. Owen, R. Pain, P. E. Palecek, J. K. Parejko, J. B. Parsons, N. M. Pease, J. M. Peterson, J. R. Peterson, D. L. Petravick, M. E. Libby Petrick, C. E. Petry, F. Pierfederici, S. Pietrowicz, R. Pike, P. A. Pinto, R. Plante, S. Plate, J. P. Plutchak, P. A. Price, M. Prouza, V. Radeka, J. Rajagopal, A. P. Rasmussen, N. Regnault, K. A. Reil, D. J. Reiss, M. A. Reuter, S. T. Ridgway, V. J. Riot, S. Ritz, S. Robinson, W. Roby, A. Roodman, W. Rosing, C. Roucelle, M. R. Rumore, S. Russo, A. Saha, B. Sassolas, T. L. Schalk, P. Schellart, R. H. Schindler, S. Schmidt, D. P. Schneider, M. D. Schneider, W. Schoening, G. Schumacher, M. E. Schwamb, J. Sebag, B. Selvy, G. H. Sembroski, L. G. Seppala, A. Serio, E. Serrano, R. A. Shaw, I. Shipsey, J. Sick, N. Silvestri, C. T. Slater, J. A. Smith, R. C. Smith, S. Sobhani, C. Soldahl, L. Storrie-Lombardi, E. Stover, M. A. Strauss, R. A. Street, C. W. Stubbs, I. S. Sullivan, D. Sweeney, J. D. Swinbank, A. Szalay, P. Takacs, S. A. Tether, J. J. Thaler, J. G. Thayer, S. Thomas, A. J. Thornton, V. Thukral, J. Tice, D. E. Trilling, M. Turri, R. Van Berg, D. Vanden Berk, K. Vetter, F. Virieux, T. Vucina, W. Wahl, L. Walkowicz, B. Walsh, C. W. Walter, D. L.

LRG sample	# of galaxies	z_{mean}	χ^2_{null}	SNR_{DM}	SNR_{null}
DR10: Outlier and photo-z correction (fiducial)					
Extended $z_{bin=1}$	856,537	0.47	27.5	15.5	5.0
Extended $z_{bin=2}$	1,422,411	0.63	49.0	19.1	6.0
Extended $z_{bin=3}$	1,951,646	0.79	80.3	26.1	8.2
Extended $z_{bin=4}$	1,690,171	0.92	34.0	14.6	4.6
Extended all	5,931,939	0.75	151.2	36.9	11.6
Main $z_{bin=1}$	374,555	0.47	23.7	14.1	4.3
Main $z_{bin=2}$	668,450	0.63	62.2	22.6	7.1
Main $z_{bin=3}$	753,945	0.79	65.9	23.4	7.3
Main $z_{bin=4}$	629,367	0.93	20.8	10.1	3.2
Main all	2,438,749	0.73	126.2	33.8	10.5
DR10: Photo-z correction only					
Extended $z_{bin=1}$	868,743	0.47	29.1	15.8	5.2
Extended $z_{bin=2}$	1,435,540	0.63	57.3	20.9	6.5
Extended $z_{bin=3}$	2,006,009	0.79	80.8	24.8	8.0
Extended $z_{bin=4}$	1,704,265	0.92	35.1	15.2	4.8
Extended all	6,014,557	0.75	164.8	38.4	12.1
Main $z_{bin=1}$	380,052	0.47	27.0	14.8	4.5
Main $z_{bin=2}$	677,185	0.63	74.0	24.4	7.7
Main $z_{bin=3}$	771,391	0.79	60.7	21.7	6.9
Main $z_{bin=4}$	636,964	0.93	20.4	10.4	3.2
Main all	2,465,593	0.73	145.4	36.0	11.2
DR10: Outlier correction only					
Extended $z_{bin=1}$	898,659	0.47	25.9	15.0	4.8
Extended $z_{bin=2}$	1,476,128	0.63	48.9	18.8	5.9
Extended $z_{bin=3}$	2,031,590	0.79	81.5	25.5	8.0
Extended $z_{bin=4}$	1,753,100	0.92	26.6	13.2	4.0
Extended all	6,174,499	0.74	142.8	35.2	11.0
Main $z_{bin=1}$	393,180	0.47	19.7	12.8	3.8
Main $z_{bin=2}$	690,663	0.63	58.2	20.5	6.5
Main $z_{bin=3}$	775,891	0.79	70.4	22.9	7.1
Main $z_{bin=4}$	645,219	0.93	20.9	9.8	3.0
Main all	2,515,452	0.73	120.7	31.9	9.9
DR10: No corrections					
Extended $z_{bin=1}$	911,407	0.47	30.2	16.6	5.3
Extended $z_{bin=2}$	1,490,492	0.63	53.9	20.1	6.2
Extended $z_{bin=3}$	2,083,198	0.79	80.8	24.2	7.8
Extended $z_{bin=4}$	1,769,651	0.92	30.0	14.4	4.4
Extended all	6,254,748	0.74	156.4	37.0	11.7
Main $z_{bin=1}$	398,735	0.47	24.0	13.8	4.1
Main $z_{bin=2}$	698,633	0.63	67.8	22.9	7.2
Main $z_{bin=3}$	790,871	0.79	62.9	21.5	6.8
Main $z_{bin=4}$	652,610	0.93	20.2	10.0	3.1
Main all	2,540,850	0.73	136.6	34.4	10.7

TABLE II. Same as Table I, but showing the effect of the different corrections applied to DR10 LRGs. The statistical significance of the measurements changes minimally.

LRG sample	# of galaxies	z_{mean}	χ^2_{null}	SNR_{DM}	SNR_{null}
DR9: Outlier and photo-z correction (fiducial)					
Extended $z_{bin=1}$	954,820	0.47	38.5	18.7	6.0
Extended $z_{bin=2}$	1,628,650	0.63	71.2	22.7	7.2
Extended $z_{bin=3}$	2,125,787	0.80	35.6	14.2	4.2
Extended $z_{bin=4}$	1,996,525	0.92	19.1	8.9	2.9
Extended all	6,697,792	0.75	98.7	29.3	9.1
Main $z_{bin=1}$	417,262	0.47	20.6	12.3	4.0
Main $z_{bin=2}$	779,408	0.63	77.4	25.0	7.9
Main $z_{bin=3}$	878,442	0.79	22.9	12.8	3.8
Main $z_{bin=4}$	765,542	0.92	12.5	8.6	2.7
Main all	2,840,853	0.74	98.2	30.0	9.4
DR9: Photo-z correction only					
Extended $z_{bin=1}$	963,631	0.47	43.2	19.9	6.4
Extended $z_{bin=2}$	1,658,313	0.63	69.4	21.6	7.1
Extended $z_{bin=3}$	2,174,053	0.80	28.5	10.9	3.4
Extended $z_{bin=4}$	2,054,075	0.92	26.2	11.2	3.8
Extended all	6,850,072	0.75	111.7	30.1	9.7
Main $z_{bin=1}$	422,350	0.47	25.2	13.7	4.4
Main $z_{bin=2}$	795,393	0.63	78.8	24.4	7.8
Main $z_{bin=3}$	888,934	0.79	23.6	11.9	3.7
Main $z_{bin=4}$	776,227	0.92	15.3	9.8	3.2
Main all	2,882,904	0.74	103.1	30.0	9.6
DR9: Outlier correction only					
Extended $z_{bin=1}$	1,065,110	0.47	37.1	18.4	5.9
Extended $z_{bin=2}$	1,775,088	0.63	73.0	20.6	6.7
Extended $z_{bin=3}$	2,331,881	0.80	32.8	14.3	4.2
Extended $z_{bin=4}$	2,386,519	0.92	33.4	12.5	3.6
Extended all	7,596,154	0.75	92.3	28.0	8.6
Main $z_{bin=1}$	464,568	0.47	18.1	11.2	3.6
Main $z_{bin=2}$	837,280	0.63	86.5	26.1	8.2
Main $z_{bin=3}$	923,974	0.79	25.1	13.6	4.1
Main $z_{bin=4}$	845,101	0.92	15.3	8.9	2.8
Main all	3,081,255	0.74	96.7	29.8	9.2
DR9: No corrections					
Extended $z_{bin=1}$	1,073,362	0.47	37.6	18.9	6.0
Extended $z_{bin=2}$	1,804,919	0.63	73.2	21.0	7.0
Extended $z_{bin=3}$	2,400,937	0.80	22.7	9.9	3.1
Extended $z_{bin=4}$	2,485,696	0.92	32.3	14.8	4.9
Extended all	7,764,914	0.75	96.9	28.3	9.0
Main $z_{bin=1}$	470,133	0.47	20.6	12.3	4.0
Main $z_{bin=2}$	854,005	0.63	85.2	25.0	8.0
Main $z_{bin=3}$	936,270	0.79	22.2	11.4	3.6
Main $z_{bin=4}$	857,753	0.92	14.8	9.3	2.9
Main all	3,118,161	0.74	95.6	28.9	9.1

TABLE III. Same as Table II, but showing DR9 instead of DR10 LRGs. We see that the statistical significance is similar to the DR10 results, but slightly reduced.

Wang, S.-Y. Wang, M. Warner, O. Wiecha, B. Willman, S. E. Winters, D. Wittman, S. C. Wolff, W. M. Wood-Vasey, X. Wu, B. Xin, P. Yoachim, and H. Zhan, LSST: From Science Drivers to Reference Design and Anticipated Data Products, ApJ **873**, 111 (2019), arXiv:0805.2366 [astro-ph].

[4] L. Amendola, S. Appleby, D. Bacon, T. Baker, M. Baldi, N. Bartolo, A. Blanchard, C. Bonvin, S. Borgani, E. Branchini, C. Burrage, S. Camera, C. Carbone, L. Casarini, M. Cropper, C. de Rham, C. Di Porto, A. Ealet, P. G. Ferreira, F. Finelli, J. García-Bellido, T. Giannantonio, L. Guzzo, A. Heavens, L. Heisenberg, C. Heymans, H. Hoekstra, L. Hollenstein, R. Holmes, O. Horst, K. Jahnke, T. D. Kitching, T. Koivisto, M. Kunz, G. La Vacca, M. March, E. Majerotto, K. Markovic, D. Marsh, F. Marulli, R. Massey, Y. Mellier, D. F. Mota, N. J. Nunes, W. Percival, V. Pettorino, C. Porciani, C. Quercellini, J. Read, M. Rinaldi, D. Sapone, R. Scaramella, C. Skordis, F. Simpson, A. Taylor, S. Thomas, R. Trotta, L. Verde, F. Vernizzi, A. Vollmer, Y. Wang, J. Weller, and T. Zlosnik, Cosmology and Fundamental Physics with the Euclid Satellite, Living Reviews in Relativity **16**, 6 (2013), arXiv:1206.1225 [astro-ph.CO].

[5] D. Spergel, N. Gehrels, C. Baltay, D. Bennett, J. Breckinridge, M. Donahue, A. Dressler, B. S. Gaudi, T. Greene, O. Guyon, C. Hirata, J. Kalirai, N. J. Kasdin, B. Macintosh, W. Moos, S. Perlmutter, M. Postman, B. Rauscher, J. Rhodes, Y. Wang, D. Weinberg, D. Benford, M. Hudson, W. S. Jeong, Y. Mellier, W. Traub, T. Yamada, P. Capak, J. Colbert, D. Masters, M. Penny, D. Savransky, D. Stern, N. Zimmerman, R. Barry, L. Bartusek, K. Carpenter, E. Cheng, D. Content, F. Dekens, R. Demers, K. Grady, C. Jackson, G. Kuan, J. Kruk, M. Melton, B. Nemati, B. Parvin, I. Poberezhskiy, C. Peddie, J. Ruffa, J. K. Wallace, A. Whipple, E. Wollack, and F. Zhao, Wide-Field InfrarRed Survey Telescope-Astrophysics Focused Telescope Assets WFIRST-AFTA 2015 Report, arXiv e-prints , arXiv:1503.03757 (2015), arXiv:1503.03757 [astro-ph.IM].

[6] R. Cen and J. P. Ostriker, Where are the baryons? II. feedback effects, The Astrophysical Journal **650**, 560 (2006).

[7] M. Birkinshaw, The Sunyaev-Zel'dovich effect, Phys. Rep. **310**, 97 (1999), arXiv:astro-ph/9808050 [astro-ph].

[8] T. Mroczkowski, D. Nagai, K. Basu, J. Chluba, J. Sayers, R. Adam, E. Churazov, A. Crites, L. Di Mascolo, D. Eckert, J. Macias-Perez, F. Mayet, L. Perotto, E. Pointecouteau, C. Romero, F. Ruppin, E. Scannapieco, and J. ZuHone, Astrophysics with the Spatially and Spectrally Resolved Sunyaev-Zeldovich Effects. A Millimetre/Submillimetre Probe of the Warm and Hot Universe, Space Sci. Rev. **215**, 17 (2019), arXiv:1811.02310 [astro-ph.CO].

[9] N. Hand, G. E. Addison, E. Aubourg, N. Battaglia, E. S. Battistelli, D. Bizyaev, J. R. Bond, H. Brewington, J. Brinkmann, B. R. Brown, S. Das, K. S. Dawson, M. J. Devlin, J. Dunkley, R. Dunner, D. J. Eisenstein, J. W. Fowler, M. B. Gralla, A. Hajian, M. Halpern, M. Hilton, A. D. Hincks, R. Hlozek, J. P. Hughes, L. Infante, K. D. Irwin, A. Kosowsky, Y.-T. Lin, E. Malanushenko, V. Malanushenko, T. A. Marriage, D. Marsden, F. Menanteau, K. Moodley, M. D. Niemack, M. R. Nolta, D. Oravetz, L. A. Page, N. Palanque-Delabrouille, K. Pan, E. D. Reese, D. J. Schlegel, D. P. Schneider, N. Sehgal, A. Shelden, J. Sievers, C. Sifón, A. Simmons, S. Snedden, D. N. Spergel, S. T. Staggs, D. S. Swetz, E. R. Switzer, H. Trac, B. A. Weaver, E. J. Wollack, C. Yeche, and C. Zunckel, Evidence of Galaxy Cluster Motions with the Kinematic Sunyaev-Zel'dovich Effect, Phys. Rev. Lett. **109**, 041101 (2012), arXiv:1203.4219 [astro-ph.CO].

[10] J. C. Hill, S. Ferraro, N. Battaglia, J. Liu, and D. N. Spergel, Kinematic Sunyaev-Zel'dovich Effect with Projected Fields: A Novel Probe of the Baryon Distribution with Planck, WMAP, and WISE Data, Phys. Rev. Lett. **117**, 051301 (2016), arXiv:1603.01608 [astro-ph.CO].

[11] S. Ferraro, J. C. Hill, N. Battaglia, J. Liu, and D. N. Spergel, Kinematic Sunyaev-Zel'dovich effect with projected fields. II. Prospects, challenges, and comparison with simulations, Phys. Rev. D **94**, 123526 (2016), arXiv:1605.02722 [astro-ph.CO].

[12] E. Schaan, S. Ferraro, M. Vargas-Magaña, K. M. Smith, S. Ho, S. Aiola, N. Battaglia, J. R. Bond, F. De Bernardis, E. Calabrese, H.-M. Cho, M. J. Devlin, J. Dunkley, P. A. Gallardo, M. Hasselfield, S. Henderson, J. C. Hill, A. D. Hincks, R. Hlozek, J. Hubmayr, J. P. Hughes, K. D. Irwin, B. Koopman, A. Kosowsky, D. Li, T. Louis, M. Lungu, M. Madhavacheril, L. Maurin, J. J. McMahon, K. Moodley, S. Naess, F. Nati, L. Newburgh, M. D. Niemack, L. A. Page, C. G. Pappas, B. Partridge, B. L. Schmitt, N. Sehgal, B. D. Sherwin, J. L. Sievers, D. N. Spergel, S. T. Staggs, A. van Engelen, E. J. Wollack, and ACTPol Collaboration, Evidence for the kinematic Sunyaev-Zel'dovich effect with the Atacama Cosmology Telescope and velocity reconstruction from the Baryon Oscillation Spectroscopic Survey, Phys. Rev. D **93**, 082002 (2016), arXiv:1510.06442 [astro-ph.CO].

[13] H. Tanimura, S. Zaroubi, and N. Aghanim, Direct detection of the kinetic Sunyaev-Zel'dovich effect in galaxy clusters, A&A **645**, A112 (2021), arXiv:2007.02952 [astro-ph.CO].

[14] E. Abdalla, G. F. Abellán, A. Aboubrahim, A. Agnello, Ö. Akarsu, Y. Akrami, G. Alestas, D. Aloni, L. Amendola, L. A. Anchordoqui, R. I. Anderson, N. Arendse, M. Asgari, M. Ballardini, V. Barger, S. Basilakos, R. C. Batista, E. S. Battistelli, R. Battye, M. Benetti, D. Benisty, A. Berlin, P. de Bernardis, E. Berti, B. Bidenko, S. Birrer, J. P. Blakeslee, K. K. Boddy, C. R. Bom, A. Bonilla, N. Borghi, F. R. Bouchet, M. Braglia, T. Buchert, E. Buckley-Geer, E. Calabrese, R. R. Caldwell, D. Camarena, S. Capozziello, S. Casertano, G. C. F. Chen, J. Chluba, A. Chen, H.-Y. Chen, A. Chudaykin, M. Cicoli, C. J. Copi, F. Courbin, F.-Y. Cyr-Racine, B. Czerny, M. Dainotti, G. D'Amico, A.-C. Davis, J. de Cruz Pérez, J. de Haro, J. Delabrouille, P. B. Denton, S. Dhawan, K. R. Dienes, E. Di Valentino, P. Du, D. Eckert, C. Escamilla-Rivera, A. Ferté, F. Finelli, P. Fosalba, W. L. Freedman, N. Frusciante, E. Gaztañaga, W. Giarè, E. Giusarma, A. Gómez-Valent, W. Handley, I. Harrison, L. Hart, D. K. Hazra, A. Heavens, A. Heinesen, H. Hildebrandt, J. C. Hill, N. B. Hogg, D. E. Holz, D. C. Hooper, N. Hosseininejad, D. Huterer, M. Ishak, M. M. Ivanov, A. H. Jaffe, I. S. Jang, K. Jedamzik, R. Jimenez, M. Joseph, S. Joudaki, M. Kamionkowski, T. Karwal, L. Kazantzidis, R. E. Keeley, M. Klasen, E. Komatsu, L. V. E. Koopmans, S. Kumar, L. Lamagna, R. Lazkoz, C.-C. Lee, J. Lesgourgues, J. Levi Said, T. R. Lewis, B. L'Huillier, M. Lucca, R. Maartens, L. M. Macri, D. Marfatia, V. Marra, C. J. A. P. Martins, S. Masi, S. Matarrese, A. Mazumdar, A. Melchiorri, O. Mena, L. Mersini-Houghton, J. Mertens, D. Milaković, Y. Minami, V. Miranda, C. Moreno-Pulido, M. Moresco, D. F. Mota, E. Mottola, S. Mozzon, J. Muir, A. Mukherjee, S. Mukherjee, P. Naselsky, P. Nath, S. Nesseris, F. Niedermann, A. Notari, R. C. Nunes, E. Ó Colgáin, K. A. Owens, E. Özülker, F. Pace, A. Paliathanasis, A. Palmese, S. Pan, D. Paoletti, S. E. Perez Bergliaffa, L. Perivolaropoulos, D. W. Pesce, V. Pettorino, O. H. E. Philcox, L. Pogosian, V. Poulin, G. Poulot, M. Raveri, M. J. Reid, F. Renzi, A. G. Riess, V. I. Sabla, P. Salucci, V. Salzano, E. N. Saridakis, B. S. Sathyaprakash, M. Schmaltz, N. Schöneberg, D. Scolnic, A. A. Sen, N. Sehgal, A. Shafieloo, M. M. Sheikh-Jabbari,

J. Silk, A. Silvestri, F. Skara, M. S. Sloth, M. Soares-Santos, J. Solà Peracaula, Y.-Y. Songsheng, J. F. Soriano, D. Staicova, G. D. Starkman, I. Szapudi, E. M. Teixeira, B. Thomas, T. Treu, E. Trott, C. van de Bruck, J. A. Vazquez, L. Verde, L. Visinelli, D. Wang, J.-M. Wang, S.-J. Wang, R. Watkins, S. Watson, J. K. Webb, N. Weiner, A. Weltman, S. J. Witte, R. Wojtak, A. K. Yadav, W. Yang, G.-B. Zhao, and M. Zumalacárregui, Cosmology intertwined: A review of the particle physics, astrophysics, and cosmology associated with the cosmological tensions and anomalies, Journal of High Energy Astrophysics **34**, 49 (2022), arXiv:2203.06142 [astro-ph.CO].

[15] A. Leauthaud, S. Saito, S. Hilbert, A. Barreira, S. More, M. White, S. Alam, P. Behroozi, K. Bundy, J. Coupon, T. Erben, C. Heymans, H. Hildebrandt, R. Mandelbaum, L. Miller, B. Moraes, M. E. S. Pereira, S. A. Rodríguez-Torres, F. Schmidt, H.-Y. Shan, M. Viel, and F. Villaescusa-Navarro, Lensing is low: cosmology, galaxy formation or new physics?, MNRAS **467**, 3024 (2017), arXiv:1611.08606 [astro-ph.CO].

[16] A. Amon, N. C. Robertson, H. Miyatake, C. Heymans, M. White, J. DeRose, S. Yuan, R. H. Wechsler, T. N. Varga, S. Bocquet, A. Dvornik, S. More, A. J. Ross, H. Hoekstra, A. Alarcon, M. Asgari, J. Blazek, A. Campos, R. Chen, A. Choi, M. Crocce, H. T. Diehl, C. Doux, K. Eckert, J. Elvin-Poole, S. Everett, A. Ferté, M. Gatti, G. Giannini, D. Gruen, R. A. Gruendl, W. G. Hartley, K. Herner, H. Hildebrandt, S. Huang, E. M. Huff, B. Joachimi, S. Lee, N. MacCrann, J. Myles, A. Navarro-Alsina, T. Nishimichi, J. Prat, L. F. Secco, I. Sevilla-Noarbe, E. Sheldon, T. Shin, T. Tröster, M. A. Troxel, I. Tutusaus, A. H. Wright, B. Yin, M. Aguena, S. Allam, J. Annis, D. Bacon, M. Bilicki, D. Brooks, D. L. Burke, A. Carnero Rosell, J. Carretero, F. J. Castander, R. Cawthon, M. Costanzi, L. N. da Costa, M. E. S. Pereira, J. de Jong, J. De Vicente, S. Desai, J. P. Dietrich, P. Doel, I. Ferrero, J. Frieman, J. García-Bellido, D. W. Gerdes, J. Gschwend, G. Gutierrez, S. R. Hinton, D. L. Hollowood, K. Honscheid, D. Huterer, A. Kannawadi, K. Kuehn, N. Kuropatkin, O. Lahav, M. Lima, M. A. G. Maia, J. L. Marshall, F. Menanteau, R. Miquel, J. J. Mohr, R. Morgan, J. Muir, F. Paz-Chinchón, A. Pieres, A. A. Plazas Malagón, A. Porredon, M. Rodriguez-Monroy, A. Roodman, E. Sanchez, S. Serrano, H. Shan, E. Suchyta, M. E. C. Swanson, G. Tarle, D. Thomas, C. To, and Y. Zhang, Consistent lensing and clustering in a low-S_8 Universe with BOSS, DES Year 3, HSC Year 1, and KiDS-1000, MNRAS **518**, 477 (2023), arXiv:2202.07440 [astro-ph.CO].

[17] DESI Collaboration, B. Abareshi, J. Aguilar, S. Ahlen, S. Alam, D. M. Alexander, R. Alfarsy, L. Allen, C. Allende Prieto, O. Alves, J. Ameel, E. Armengaud, J. Asorey, A. Aviles, S. Bailey, A. Balaguera-Antolínez, O. Ballester, C. Baltay, A. Bault, S. F. Beltran, B. Benavides, S. BenZvi, A. Berti, R. Besuner, F. Beutler, D. Bianchi, C. Blake, P. Blanc, R. Blum, A. Bolton, S. Bose, D. Bramall, S. Brieden, A. Brodzeller, D. Brooks, C. Brownewell, E. Buckley-Geer, R. N. Cahn, Z. Cai, R. Canning, R. Capasso, A. Carnero Rosell, P. Carton, R. Casas, F. J. Castander, J. L. Cervantes-Cota, S. Chabanier, E. Chaussidon, C. Chuang, C. Circosta, S. Cole, A. P. Cooper, L. da Costa, M. C. Cousinou, A. Cuceu, T. M. Davis, K. Dawson, R. de la Cruz-Noriega, A. de la Macorra, A. de Mattia, J. Della Costa, P. Demmer, M. Derwent, A. Dey, B. Dey, G. Dhungana, Z. Ding, C. Dobson, P. Doel, J. Donald-McCann, J. Donaldson, K. Douglass, Y. Duan, P. Dunlop, J. Edelstein, S. Eftekharzadeh, D. J. Eisenstein, M. Enriquez-Vargas, S. Escoffier, M. Evatt, P. Fagrelius, X. Fan, K. Fanning, V. A. Fawcett, S. Ferraro, J. Ereza, B. Flaugher, A. Font-Ribera, J. E. Forero-Romero, C. S. Frenk, S. Fromenteau, B. T. Gänsicke, C. Garcia-Quintero, L. Garrison, E. Gaztañaga, F. Gerardi, H. Gil-Marín, S. Gontcho a Gontcho, A. X. Gonzalez-Morales, G. Gonzalez-de-Rivera, V. Gonzalez-Perez, C. Gordon, O. Graur, D. Green, C. Grove, D. Gruen, G. Gutierrez, J. Guy, C. Hahn, S. Harris, D. Herrera, H. K. Herrera-Alcantar, K. Honscheid, C. Howlett, D. Huterer, V. Iršič, M. Ishak, P. Jelinsky, L. Jiang, J. Jimenez, Y. P. Jing, R. Joyce, E. Jullo, S. Juneau, N. G. Karaçaylı, M. Karamanis, A. Karcher, T. Karim, R. Kehoe, S. Kent, D. Kirkby, T. Kisner, F. Kitaura, S. E. Koposov, A. Kovács, A. Kremin, A. Krolewski, B. L'Huillier, O. Lahav, A. Lambert, C. Lamman, T.-W. Lan, M. Landriau, S. Lane, D. Lang, J. U. Lange, J. Lasker, L. Le Guillou, A. Leauthaud, A. Le Van Suu, M. E. Levi, T. S. Li, C. Magneville, M. Manera, C. J. Manser, B. Marshall, P. Martini, W. McCollam, P. McDonald, A. M. Meisner, J. Mena-Fernández, J. Meneses-Rizo, M. Mezcua, T. Miller, R. Miquel, P. Montero-Camacho, J. Moon, J. Moustakas, E. Mueller, A. Muñoz-Gutiérrez, A. D. Myers, S. Nadathur, J. Najita, L. Napolitano, E. Neilsen, J. A. Newman, J. D. Nie, Y. Ning, G. Niz, P. Norberg, H. E. Noriega, T. O'Brien, A. Obuljen, N. Palanque-Delabrouille, A. Palmese, P. Zhiwei, D. Pappalardo, X. PENG, W. J. Percival, S. Perruchot, R. Pogge, C. Poppett, A. Porredon, F. Prada, J. Prochaska, R. Pucha, A. Pérez-Fernández, I. Pérez-Ràfols, D. Rabinowitz, A. Raichoor, S. Ramirez-Solano, C. Ramírez-Pérez, C. Ravoux, K. Reil, M. Rezaie, A. Rocher, C. Rockosi, N. A. Roe, A. Roodman, A. J. Ross, G. Rossi, R. Ruggeri, V. Ruhlmann-Kleider, C. G. Sabiu, S. Safonova, K. Said, A. Saintonge, J. Salas Catonga, L. Samushia, E. Sanchez, C. Saulder, E. Schaan, E. Schlafly, D. Schlegel, J. Schmoll, D. Scholte, M. Schubnell, A. Secroun, H. Seo, S. Serrano, R. M. Sharples, M. J. Sholl, J. H. Silber, D. R. Silva, M. Sirk, M. Siudek, A. Smith, D. Sprayberry, R. Staten, B. Stupak, T. Tan, G. Tarlé, S. S. Tie, R. Tojeiro, L. A. Ureña-López, F. Valdes, O. Valenzuela, M. Valluri, M. Vargas-Magaña, L. Verde, M. Walther, B. Wang, M. S. Wang, B. A. Weaver, C. Weaverdyck, R. Wechsler, M. J. Wilson, J. Yang, Y. Yu, S. Yuan, C. Yèche, H. Zhang, K. Zhang, C. Zhao, R. Zhou, Z. Zhou, H. Zou, J. Zou, S. Zou, Y. Zu, and DESI Collaboration, Overview of the Instrumentation for the Dark Energy Spectroscopic Instrument, AJ **164**, 207 (2022), arXiv:2205.10939 [astro-ph.IM].

[18] DESI Collaboration, A. Aghamousa, J. Aguilar, S. Ahlen, S. Alam, L. E. Allen, C. Allende Prieto, J. Annis, S. Bailey, C. Balland, O. Ballester, C. Baltay, L. Beaufore, C. Bebek, T. C. Beers, E. F. Bell, J. L. Bernal, R. Besuner, F. Beutler, C. Blake, H. Bleuler, M. Blomqvist, R. Blum, A. S. Bolton, C. Briceno, D. Brooks, J. R. Brownstein, E. Buckley-Geer, A. Burden, E. Burtin, N. G. Busca, R. N. Cahn, Y.-C. Cai, L. Cardiel-Sas, R. G. Carlberg, P.-H. Carton, R. Casas, F. J. Castander, J. L. Cervantes-Cota, T. M. Claybaugh, M. Close, C. T. Coker, S. Cole, J. Comparat, A. P. Cooper, M. C. Cousinou, M. Crocce, J.-G. Cuby, D. P. Cunningham, T. M. Davis, K. S. Dawson, A. de la Macorra, J. De Vicente, T. Delubac, M. Derwent, A. Dey, G. Dhungana, Z. Ding, P. Doel, Y. T. Duan, A. Ealet, J. Edelstein, S. Eftekharzadeh, D. J. Eisenstein, A. Elliott, S. Escoffier, M. Evatt, P. Fagrelius, X. Fan, K. Fanning, A. Farahi, J. Farihi, G. Favole, Y. Feng, E. Fernandez, J. R. Findlay, D. P. Finkbeiner, M. J. Fitzpatrick, B. Flaugher, S. Flender, A. Font-Ribera, J. E. Forero-Romero, P. Fosalba, C. S. Frenk, M. Fumagalli, B. T. Gaensicke, G. Gallo, J. Garcia-Bellido, E. Gaztanaga, N. Pietro Gentile Fusillo, T. Gerard, I. Gershkovich, T. Giannantonio, D. Gillet, G. Gonzalez-de-Rivera, V. Gonzalez-Perez, S. Gott, O. Graur, G. Gutierrez, J. Guy, S. Habib, H. Heetderks, I. Heetderks, K. Heitmann, W. A. Hellwing, D. A. Herrera, S. Ho, S. Holland, K. Hon-

scheid, E. Huff, T. A. Hutchinson, D. Huterer, H. S. Hwang, J. M. Illa Laguna, Y. Ishikawa, D. Jacobs, N. Jeffrey, P. Jelinsky, E. Jennings, L. Jiang, J. Jimenez, J. Johnson, R. Joyce, E. Jullo, S. Juneau, S. Kama, A. Karcher, S. Karkar, R. Kehoe, N. Kennamer, S. Kent, M. Kilbinger, A. G. Kim, D. Kirkby, T. Kisner, E. Kitanidis, J.-P. Kneib, S. Koposov, E. Kovacs, K. Koyama, A. Kremin, R. Kron, L. Kronig, A. Kueter-Young, C. G. Lacey, R. Lafever, O. Lahav, A. Lambert, M. Lampton, M. Landriau, D. Lang, T. R. Lauer, J.-M. Le Goff, L. Le Guillou, A. Le Van Suu, J. H. Lee, S.-J. Lee, D. Leitner, M. Lesser, M. E. Levi, B. L'Huillier, B. Li, M. Liang, H. Lin, E. Linder, S. R. Loebman, Z. Lukić, J. Ma, N. MacCrann, C. Magneville, L. Makarem, M. Manera, C. J. Manser, R. Marshall, P. Martini, R. Massey, T. Matheson, J. McCauley, P. McDonald, I. D. McGreer, A. Meisner, N. Metcalfe, T. N. Miller, R. Miquel, J. Moustakas, A. Myers, M. Naik, J. A. Newman, R. C. Nichol, A. Nicola, L. Nicolati da Costa, J. Nie, G. Niz, P. Norberg, B. Nord, D. Norman, P. Nugent, T. O'Brien, M. Oh, K. A. G. Olsen, C. Padilla, H. Padmanabhan, N. Padmanabhan, N. Palanque-Delabrouille, A. Palmese, D. Pappalardo, I. Pâris, C. Park, A. Patej, J. A. Peacock, H. V. Peiris, X. Peng, W. J. Percival, S. Perruchot, M. M. Pieri, R. Pogge, J. E. Pollack, C. Poppett, F. Prada, A. Prakash, R. G. Probst, D. Rabinowitz, A. Raichoor, C. H. Ree, A. Refregier, X. Regal, B. Reid, K. Reil, M. Rezaie, C. M. Rockosi, N. Roe, S. Ronayette, A. Roodman, A. J. Ross, N. P. Ross, G. Rossi, E. Rozo, V. Ruhlmann-Kleider, E. S. Rykoff, C. Sabiu, L. Samushia, E. Sanchez, J. Sanchez, D. J. Schlegel, M. Schneider, M. Schubnell, A. Secroun, U. Seljak, H.-J. Seo, S. Serrano, A. Shafieloo, H. Shan, R. Sharples, M. J. Sholl, W. V. Shourt, J. H. Silber, D. R. Silva, M. M. Sirk, A. Slosar, A. Smith, G. F. Smoot, D. Som, Y.-S. Song, D. Sprayberry, R. Staten, A. Stefanik, G. Tarle, S. Sien Tie, J. L. Tinker, R. Tojeiro, F. Valdes, O. Valenzuela, M. Valluri, M. Vargas-Magana, L. Verde, A. R. Walker, J. Wang, Y. Wang, B. A. Weaver, C. Weaverdyck, R. H. Wechsler, D. H. Weinberg, M. White, Q. Yang, C. Yeche, T. Zhang, G.-B. Zhao, Y. Zheng, X. Zhou, Z. Zhou, Y. Zhu, H. Zou, and Y. Zu, The DESI Experiment Part II: Instrument Design, arXiv e-prints , arXiv:1611.00037 (2016), arXiv:1611.00037 [astro-ph.IM].

[19] J. H. Silber, P. Fagrelius, K. Fanning, M. Schubnell, J. N. Aguilar, S. Ahlen, J. Ameel, O. Ballester, C. Baltay, C. Bebek, D. Benton Beard, R. Besuner, L. Cardiel-Sas, R. Casas, F. J. Castander, T. Claybaugh, C. Dobson, Y. Duan, P. Dunlop, J. Edelstein, W. T. Emmet, A. Elliott, M. Evatt, I. Gershkovich, J. Guy, S. Harris, H. Heetderks, I. Heetderks, K. Honscheid, J. M. Illa, P. Jelinsky, S. R. Jelinsky, J. Jimenez, A. Karcher, S. Kent, D. Kirkby, J.-P. Kneib, A. Lambert, M. Lampton, D. Leitner, M. Levi, J. McCauley, A. Meisner, T. N. Miller, R. Miquel, J. Mundet, C. Poppett, D. Rabinowitz, K. Reil, D. Roman, D. Schlegel, S. Serrano, W. Van Shourt, D. Sprayberry, G. Tarlé, S. S. Tie, C. Weaverdyck, K. Zhang, M. Azzaro, S. Bailey, S. Becerril, T. Blackwell, M. Bouri, D. Brooks, E. Buckley-Geer, J. P. Castro, M. Derwent, A. Dey, G. Dhungana, P. Doel, D. J. Eisenstein, N. Fahim, J. Garcia-Bellido, E. Gaztañaga, S. G. A Gontcho, G. Gutierrez, P. Hörler, R. Kehoe, T. Kisner, A. Kremin, L. Kronig, M. Landriau, L. Le Guillou, P. Martini, J. Moustakas, N. Palanque-Delabrouille, X. Peng, W. Percival, F. Prada, C. Allende Prieto, G. G. de Rivera, E. Sanchez, J. Sanchez, R. Sharples, M. Soares-Santos, E. Schlafly, B. A. Weaver, Z. Zhou, Y. Zhu, H. Zou, and DESI Collaboration, The Robotic Multiobject Focal Plane System of the Dark Energy Spectroscopic Instrument (DESI), AJ **165**, 9 (2023), arXiv:2205.09014 [astro-ph.IM].

[20] T. N. Miller, P. Doel, G. Gutierrez, R. Besuner, D. Brooks, G. Gallo, H. Heetderks, P. Jelinsky, S. M. Kent, M. Lampton, M. Levi, M. Liang, A. Meisner, M. J. Sholl, J. H. Silber, D. Sprayberry, J. N. Aguilar, A. de la Macorra, D. Eisenstein, K. Fanning, A. Font-Ribera, E. Gaztanaga, S. G. A. Gontcho, K. Honscheid, J. Jimenez, D. Joyce, R. Kehoe, T. Kisner, A. Kremin, M. Landriau, L. Le Guillou, C. Magneville, P. Martini, R. Miquel, J. Moustakas, J. Nie, W. Percival, C. Poppett, F. Prada, G. Rossi, D. Schlegel, M. Schubnell, H.-J. Seo, R. Sharples, G. Tarle, M. Vargas-Magana, and Z. Zhou, The Optical Corrector for the Dark Energy Spectroscopic Instrument, arXiv e-prints , arXiv:2306.06310 (2023), arXiv:2306.06310 [astro-ph.IM].

[21] M. Levi, C. Bebek, T. Beers, R. Blum, R. Cahn, D. Eisenstein, B. Flaugher, K. Honscheid, R. Kron, O. Lahav, P. McDonald, N. Roe, D. Schlegel, and representing the DESI collaboration, The DESI Experiment, a whitepaper for Snowmass 2013, arXiv e-prints , arXiv:1308.0847 (2013), arXiv:1308.0847 [astro-ph.CO].

[22] DESI Collaboration, A. Aghamousa, J. Aguilar, S. Ahlen, S. Alam, L. E. Allen, C. Allende Prieto, J. Annis, S. Bailey, C. Balland, O. Ballester, C. Baltay, L. Beaufore, C. Bebek, T. C. Beers, E. F. Bell, J. L. Bernal, R. Besuner, F. Beutler, C. Blake, H. Bleuler, M. Blomqvist, R. Blum, A. S. Bolton, C. Briceno, D. Brooks, J. R. Brownstein, E. Buckley-Geer, A. Burden, E. Burtin, N. G. Busca, R. N. Cahn, Y.-C. Cai, L. Cardiel-Sas, R. G. Carlberg, P.-H. Carton, R. Casas, F. J. Castander, J. L. Cervantes-Cota, T. M. Claybaugh, M. Close, C. T. Coker, S. Cole, J. Comparat, A. P. Cooper, M. C. Cousinou, M. Crocce, J.-G. Cuby, D. P. Cunningham, T. M. Davis, K. S. Dawson, A. de la Macorra, J. De Vicente, T. Delubac, M. Derwent, A. Dey, G. Dhungana, Z. Ding, P. Doel, Y. T. Duan, A. Ealet, J. Edelstein, S. Eftekharzadeh, D. J. Eisenstein, A. Elliott, S. Escoffier, M. Evatt, P. Fagrelius, X. Fan, K. Fanning, A. Farahi, J. Farihi, G. Favole, Y. Feng, E. Fernandez, J. R. Findlay, D. P. Finkbeiner, M. J. Fitzpatrick, B. Flaugher, S. Flender, A. Font-Ribera, J. E. Forero-Romero, P. Fosalba, C. S. Frenk, M. Fumagalli, B. T. Gaensicke, G. Gallo, J. Garcia-Bellido, E. Gaztanaga, N. Pietro Gentile Fusillo, T. Gerard, I. Gershkovich, T. Giannantonio, D. Gillet, G. Gonzalez-de-Rivera, V. Gonzalez-Perez, S. Gott, O. Graur, G. Gutierrez, J. Guy, S. Habib, H. Heetderks, I. Heetderks, K. Heitmann, W. A. Hellwing, D. A. Herrera, S. Ho, S. Holland, K. Honscheid, E. Huff, T. A. Hutchinson, D. Huterer, H. S. Hwang, J. M. Illa Laguna, Y. Ishikawa, D. Jacobs, N. Jeffrey, P. Jelinsky, E. Jennings, L. Jiang, J. Jimenez, J. Johnson, R. Joyce, E. Jullo, S. Juneau, S. Kama, A. Karcher, S. Karkar, R. Kehoe, N. Kennamer, S. Kent, M. Kilbinger, A. G. Kim, D. Kirkby, T. Kisner, E. Kitanidis, J.-P. Kneib, S. Koposov, E. Kovacs, K. Koyama, A. Kremin, R. Kron, L. Kronig, A. Kueter-Young, C. G. Lacey, R. Lafever, O. Lahav, A. Lambert, M. Lampton, M. Landriau, D. Lang, T. R. Lauer, J.-M. Le Goff, L. Le Guillou, A. Le Van Suu, J. H. Lee, S.-J. Lee, D. Leitner, M. Lesser, M. E. Levi, B. L'Huillier, B. Li, M. Liang, H. Lin, E. Linder, S. R. Loebman, Z. Lukić, J. Ma, N. MacCrann, C. Magneville, L. Makarem, M. Manera, C. J. Manser, R. Marshall, P. Martini, R. Massey, T. Matheson, J. McCauley, P. McDonald, I. D. McGreer, A. Meisner, N. Metcalfe, T. N. Miller, R. Miquel, J. Moustakas, A. Myers, M. Naik, J. A. Newman, R. C. Nichol, A. Nicola, L. Nicolati da Costa, J. Nie, G. Niz, P. Norberg, B. Nord, D. Norman, P. Nugent, T. O'Brien, M. Oh, K. A. G. Olsen, C. Padilla, H. Padmanabhan, N. Padmanabhan, N. Palanque-Delabrouille, A. Palmese, D. Pappalardo, I. Pâris, C. Park, A. Patej, J. A. Peacock, H. V. Peiris, X. Peng, W. J. Percival, S. Perruchot, M. M. Pieri, R. Pogge, J. E. Pollack,

C. Poppett, F. Prada, A. Prakash, R. G. Probst, D. Rabinowitz, A. Raichoor, C. H. Ree, A. Refregier, X. Regal, B. Reid, K. Reil, M. Rezaie, C. M. Rockosi, N. Roe, S. Ronayette, A. Roodman, A. J. Ross, N. P. Ross, G. Rossi, E. Rozo, V. Ruhlmann-Kleider, E. S. Rykoff, C. Sabiu, L. Samushia, E. Sanchez, J. Sanchez, D. J. Schlegel, M. Schneider, M. Schubnell, A. Secroun, U. Seljak, H.-J. Seo, S. Serrano, A. Shafieloo, H. Shan, R. Sharples, M. J. Sholl, W. V. Shourt, J. H. Silber, D. R. Silva, M. M. Sirk, A. Slosar, A. Smith, G. F. Smoot, D. Som, Y.-S. Song, D. Sprayberry, R. Staten, A. Stefanik, G. Tarle, S. Sien Tie, J. L. Tinker, R. Tojeiro, F. Valdes, O. Valenzuela, M. Valluri, M. Vargas-Magana, L. Verde, A. R. Walker, J. Wang, Y. Wang, B. A. Weaver, C. Weaverdyck, R. H. Wechsler, D. H. Weinberg, M. White, Q. Yang, C. Yeche, T. Zhang, G.-B. Zhao, Y. Zheng, X. Zhou, Z. Zhou, Y. Zhu, H. Zou, and Y. Zu, The DESI Experiment Part I: Science,Targeting, and Survey Design, arXiv e-prints , arXiv:1611.00036 (2016), arXiv:1611.00036 [astro-ph.IM].

[23] H. Zou, X. Zhou, X. Fan, T. Zhang, Z. Zhou, J. Nie, X. Peng, I. McGreer, L. Jiang, A. Dey, D. Fan, B. He, Z. Jiang, D. Lang, M. Lesser, J. Ma, S. Mao, D. Schlegel, and J. Wang, Project Overview of the Beijing-Arizona Sky Survey, PASP **129**, 064101 (2017), arXiv:1702.03653 [astro-ph.GA].

[24] A. Dey, D. J. Schlegel, D. Lang, R. Blum, K. Burleigh, X. Fan, J. R. Findlay, D. Finkbeiner, D. Herrera, S. Juneau, M. Landriau, M. Levi, I. McGreer, A. Meisner, A. D. Myers, J. Moustakas, P. Nugent, A. Patej, E. F. Schlafly, A. R. Walker, F. Valdes, B. A. Weaver, C. Yèche, H. Zou, X. Zhou, B. Abareshi, T. M. C. Abbott, B. Abolfathi, C. Aguilera, S. Alam, L. Allen, A. Alvarez, J. Annis, B. Ansarinejad, M. Aubert, J. Beechert, E. F. Bell, S. Y. BenZvi, F. Beutler, R. M. Bielby, A. S. Bolton, C. Briceño, E. J. Buckley-Geer, K. Butler, A. Calamida, R. G. Carlberg, P. Carter, R. Casas, F. J. Castander, Y. Choi, J. Comparat, E. Cukanovaite, T. Delubac, K. DeVries, S. Dey, G. Dhungana, M. Dickinson, Z. Ding, J. B. Donaldson, Y. Duan, C. J. Duckworth, S. Eftekharzadeh, D. J. Eisenstein, T. Etourneau, P. A. Fagrelius, J. Farihi, M. Fitzpatrick, A. Font-Ribera, L. Fulmer, B. T. Gänsicke, E. Gaztanaga, K. George, D. W. Gerdes, S. G. A. Gontcho, C. Gorgoni, G. Green, J. Guy, D. Harmer, M. Hernandez, K. Honscheid, L. W. Huang, D. J. James, B. T. Jannuzi, L. Jiang, R. Joyce, A. Karcher, S. Karkar, R. Kehoe, J.-P. Kneib, A. Kueter-Young, T.-W. Lan, T. R. Lauer, L. Le Guillou, A. Le Van Suu, J. H. Lee, M. Lesser, L. Perreault Levasseur, T. S. Li, J. L. Mann, R. Marshall, C. E. Martínez-Vázquez, P. Martini, H. du Mas des Bourboux, S. McManus, T. G. Meier, B. Ménard, N. Metcalfe, A. Muñoz-Gutiérrez, J. Najita, K. Napier, G. Narayan, J. A. Newman, J. Nie, B. Nord, D. J. Norman, K. A. G. Olsen, A. Paat, N. Palanque-Delabrouille, X. Peng, C. L. Poppett, M. R. Poremba, A. Prakash, D. Rabinowitz, A. Raichoor, M. Rezaie, A. N. Robertson, N. A. Roe, A. J. Ross, N. P. Ross, G. Rudnick, S. Safonova, A. Saha, F. J. Sánchez, E. Savary, H. Schweiker, A. Scott, H.-J. Seo, H. Shan, D. R. Silva, Z. Slepian, C. Soto, D. Sprayberry, R. Staten, C. M. Stillman, R. J. Stupak, D. L. Summers, S. Sien Tie, H. Tirado, M. Vargas-Magaña, A. K. Vivas, R. H. Wechsler, D. Williams, J. Yang, Q. Yang, T. Yapici, D. Zaritsky, A. Zenteno, K. Zhang, T. Zhang, R. Zhou, and Z. Zhou, Overview of the DESI Legacy Imaging Surveys, AJ **157**, 168 (2019), arXiv:1804.08657 [astro-ph.IM].

[25] R. Zhou, J. A. Newman, K. S. Dawson, D. J. Eisenstein, D. D. Brooks, A. Dey, B. Dey, Y. Duan, S. Eftekharzadeh, E. Gaztañaga, R. Kehoe, M. Landriau, M. E. Levi, T. C. Licquia, A. M. Meisner, J. Moustakas, A. D. Myers, N. Palanque-Delabrouille, C. Poppett, F. Prada, A. Raichoor, D. J. Schlegel, M. Schubnell, R. Staten, G. Tarlé, and C. Yèche, Preliminary Target Selection for the DESI Luminous Red Galaxy (LRG) Sample, Research Notes of the American Astronomical Society **4**, 181 (2020), arXiv:2010.11282 [astro-ph.CO].

[26] R. Zhou, B. Dey, J. A. Newman, D. J. Eisenstein, K. Dawson, S. Bailey, A. Berti, J. Guy, T.-W. Lan, H. Zou, J. Aguilar, S. Ahlen, S. Alam, D. Brooks, A. de la Macorra, A. Dey, G. Dhungana, K. Fanning, A. Font-Ribera, S. G. A. Gontcho, K. Honscheid, M. Ishak, T. Kisner, A. Kovács, A. Kremin, M. Landriau, M. E. Levi, C. Magneville, M. Manera, P. Martini, A. M. Meisner, R. Miquel, J. Moustakas, A. D. Myers, J. Nie, N. Palanque-Delabrouille, W. J. Percival, C. Poppett, F. Prada, A. Raichoor, A. J. Ross, E. Schlafly, D. Schlegel, M. Schubnell, G. Tarlé, B. A. Weaver, R. H. Wechsler, C. Yéche, and Z. Zhou, Target Selection and Validation of DESI Luminous Red Galaxies, AJ **165**, 58 (2023), arXiv:2208.08515 [astro-ph.CO].

[27] R. Zhou, S. Ferraro, M. White, J. DeRose, N. Sailer, J. Aguilar, S. Ahlen, S. Bailey, D. Brooks, T. Claybaugh, K. Dawson, A. de la Macorra, B. Dey, P. Doel, A. Font-Ribera, J. E. Forero-Romero, S. Gontcho A Gontcho, J. Guy, A. Kremin, A. Lambert, L. Le Guillou, M. Levi, C. Magneville, M. Manera, A. Meisner, R. Miquel, J. Moustakas, A. D. Myers, J. A. Newman, J. Nie, W. Percival, M. Rezaie, G. Rossi, E. Sanchez, D. Schlegel, M. Schubnell, H.-J. Seo, G. Tarlé, and Z. Zhou, DESI luminous red galaxy samples for cross-correlations, J. Cosmology Astropart. Phys. **2023**, 097 (2023), arXiv:2309.06443 [astro-ph.CO].

[28] B. Hadzhiyska, S. Ferraro, B. Ried Guachalla, and E. Schaan, Velocity reconstruction in the era of DESI and Rubin/LSST. II. Realistic samples on the light cone, Phys. Rev. D **109**, 103534 (2024), arXiv:2312.12434 [astro-ph.CO].

[29] W. Coulton, M. S. Madhavacheril, A. J. Duivenvoorden, J. C. Hill, I. Abril-Cabezas, P. A. R. Ade, S. Aiola, T. Alford, M. Amiri, S. Amodeo, R. An, Z. Atkins, J. E. Austermann, N. Battaglia, E. S. Battistelli, J. A. Beall, R. Bean, B. Beringue, T. Bhandarkar, E. Biermann, B. Bolliet, J. R. Bond, H. Cai, E. Calabrese, V. Calafut, V. Capalbo, F. Carrero, G. E. Chesmore, H.-m. Cho, S. K. Choi, S. E. Clark, R. C. Rosado, N. F. Cothard, K. Coughlin, K. T. Crowley, M. J. Devlin, S. Dicker, P. Doze, C. J. Duell, S. M. Duff, J. Dunkley, R. Dünner, V. Fanfani, M. Fankhanel, G. Farren, S. Ferraro, R. Freundt, B. Fuzia, P. A. Gallardo, X. Garrido, J. Givans, V. Gluscevic, J. E. Golec, Y. Guan, M. Halpern, D. Han, M. Hasselfield, E. Healy, S. Henderson, B. Hensley, C. Hervías-Caimapo, G. C. Hilton, M. Hilton, A. D. Hincks, R. Hložek, S.-P. P. Ho, Z. B. Huber, J. Hubmayr, K. M. Huffenberger, J. P. Hughes, K. Irwin, G. Isopi, H. T. Jense, B. Keller, J. Kim, K. Knowles, B. J. Koopman, A. Kosowsky, D. Kramer, A. Kusiak, A. La Posta, V. Lakey, E. Lee, Z. Li, Y. Li, M. Limon, M. Lokken, T. Louis, M. Lungu, N. MacCrann, A. MacInnis, D. Maldonado, F. Maldonado, M. Mallaby-Kay, G. A. Marques, J. van Marrewijk, F. McCarthy, J. McMahon, Y. Mehta, F. Menanteau, K. Moodley, T. W. Morris, T. Mroczkowski, S. Naess, T. Namikawa, F. Nati, L. Newburgh, A. Nicola, M. D. Niemack, M. R. Nolta, J. Orlowski-Scherer, L. A. Page, S. Pandey, B. Partridge, H. Prince, R. Puddu, F. J. Qu, F. Radiconi, N. Robertson, F. Rojas, T. Sakuma, M. Salatino, E. Schaan, B. L. Schmitt, N. Sehgal, S. Shaikh, B. D. Sherwin, C. Sierra, J. Sievers, C. Sifón, S. Simon, R. Sonka, D. N. Spergel, S. T. Staggs, E. Storer, E. R. Switzer, N. Tampier, R. Thornton, H. Trac, J. Treu, C. Tucker, J. Ullom, L. R. Vale, A. Van Engelen, J. Van Lanen, C. Vargas, E. M. Vavagiakis, K. Wagoner, Y. Wang, L. Wenzl, E. J. Wollack, Z. Xu, F. Zago, and K. Zheng, Atacama Cosmology Telescope: High-resolution component-separated

maps across one third of the sky, Phys. Rev. D **109**, 063530 (2024), arXiv:2307.01258 [astro-ph.CO].

[30] S. Naess, S. Aiola, J. E. Austermann, N. Battaglia, J. A. Beall, D. T. Becker, R. J. Bond, E. Calabrese, S. K. Choi, N. F. Cothard, K. T. Crowley, O. Darwish, R. Datta, E. V. Denison, M. Devlin, C. J. Duell, S. M. Duff, A. J. Duivenvoorden, J. Dunkley, R. Dünner, A. E. Fox, P. A. Gallardo, M. Halpern, D. Han, M. Hasselfield, J. C. Hill, G. C. Hilton, M. Hilton, A. D. Hincks, R. Hložek, S.-P. P. Ho, J. Hubmayr, K. Huffenberger, J. P. Hughes, A. B. Kosowsky, T. Louis, M. S. Madhavacheril, J. McMahon, K. Moodley, F. Nati, J. P. Nibarger, M. D. Niemack, L. Page, B. Partridge, M. Salatino, E. Schaan, A. Schillaci, B. Schmitt, B. D. Sherwin, N. Sehgal, C. Sifón, D. Spergel, S. Staggs, J. Stevens, E. Storer, J. N. Ullom, L. R. Vale, A. Van Engelen, J. Van Lanen, E. M. Vavagiakis, E. J. Wollack, and Z. Xu, The Atacama Cosmology Telescope: arcminute-resolution maps of 18 000 square degrees of the microwave sky from ACT 2008-2018 data combined with Planck, J. Cosmology Astropart. Phys. **2020**, 046 (2020), arXiv:2007.07290 [astro-ph.IM].

[31] R. J. Thornton, P. A. R. Ade, S. Aiola, F. E. Angilè, M. Amiri, J. A. Beall, D. T. Becker, H. M. Cho, S. K. Choi, P. Corlies, K. P. Coughlin, R. Datta, M. J. Devlin, S. R. Dicker, R. Dünner, J. W. Fowler, A. E. Fox, P. A. Gallardo, J. Gao, E. Grace, M. Halpern, M. Hasselfield, S. W. Henderson, G. C. Hilton, A. D. Hincks, S. P. Ho, J. Hubmayr, K. D. Irwin, J. Klein, B. Koopman, D. Li, T. Louis, M. Lungu, L. Maurin, J. McMahon, C. D. Munson, S. Naess, F. Nati, L. Newburgh, J. Nibarger, M. D. Niemack, P. Niraula, M. R. Nolta, L. A. Page, C. G. Pappas, A. Schillaci, B. L. Schmitt, N. Sehgal, J. L. Sievers, S. M. Simon, S. T. Staggs, C. Tucker, M. Uehara, J. van Lanen, J. T. Ward, and E. J. Wollack, The Atacama Cosmology Telescope: The Polarization-sensitive ACTPol Instrument, ApJS **227**, 21 (2016), arXiv:1605.06569 [astro-ph.IM].

[32] M. S. Madhavacheril, F. J. Qu, B. D. Sherwin, N. MacCrann, Y. Li, I. Abril-Cabezas, P. A. R. Ade, S. Aiola, T. Alford, M. Amiri, S. Amodeo, R. An, Z. Atkins, J. E. Austermann, N. Battaglia, E. S. Battistelli, J. A. Beall, R. Bean, B. Beringue, T. Bhandarkar, E. Biermann, B. Bolliet, J. R. Bond, H. Cai, E. Calabrese, V. Calafut, V. Capalbo, F. Carrero, A. Challinor, G. E. Chesmore, H.-m. Cho, S. K. Choi, S. E. Clark, R. Córdova Rosado, N. F. Cothard, K. Coughlin, W. Coulton, K. T. Crowley, R. Dalal, O. Darwish, M. J. Devlin, S. Dicker, P. Doze, C. J. Duell, S. M. Duff, A. J. Duivenvoorden, J. Dunkley, R. Dünner, V. Fanfani, M. Fankhanel, G. Farren, S. Ferraro, R. Freundt, B. Fuzia, P. A. Gallardo, X. Garrido, J. Givans, V. Gluscevic, J. E. Golec, Y. Guan, K. R. Hall, M. Halpern, D. Han, I. Harrison, M. Hasselfield, E. Healy, S. Henderson, B. Hensley, C. Hervías-Caimapo, J. C. Hill, G. C. Hilton, M. Hilton, A. D. Hincks, R. Hložek, S.-P. P. Ho, Z. B. Huber, J. Hubmayr, K. M. Huffenberger, J. P. Hughes, K. Irwin, G. Isopi, H. T. Jense, B. Keller, J. Kim, K. Knowles, B. J. Koopman, A. Kosowsky, D. Kramer, A. Kusiak, A. La Posta, A. Lague, V. Lakey, E. Lee, Z. Li, M. Limon, M. Lokken, T. Louis, M. Lungu, A. MacInnis, D. Maldonado, F. Maldonado, M. Mallaby-Kay, G. A. Marques, J. McMahon, Y. Mehta, F. Menanteau, K. Moodley, T. W. Morris, T. Mroczkowski, S. Naess, T. Namikawa, F. Nati, L. Newburgh, A. Nicola, M. D. Niemack, M. R. Nolta, J. Orlowski-Scherer, L. A. Page, S. Pandey, B. Partridge, H. Prince, R. Puddu, F. Radiconi, N. Robertson, F. Rojas, T. Sakuma, M. Salatino, E. Schaan, B. L. Schmitt, N. Sehgal, S. Shaikh, C. Sierra, J. Sievers, C. Sifón, S. Simon, R. Sonka, D. N. Spergel, S. T. Staggs, E. Storer, E. R. Switzer, N. Tampier, R. Thornton, H. Trac, J. Treu, C. Tucker, J. Ullom, L. R. Vale, A. Van Engelen, J. Van Lanen, J. van Marrewijk, C. Vargas, E. M. Vavagiakis, K. Wagoner, Y. Wang, L. Wenzl, E. J. Wollack, Z. Xu, F. Zago, and K. Zheng, The Atacama Cosmology Telescope: DR6 Gravitational Lensing Map and Cosmological Parameters, ApJ **962**, 113 (2024), arXiv:2304.05203 [astro-ph.CO].

[33] E. Schaan, S. Ferraro, S. Amodeo, N. Battaglia, S. Aiola, J. E. Austermann, J. A. Beall, R. Bean, D. T. Becker, R. J. Bond, E. Calabrese, V. Calafut, S. K. Choi, E. V. Denison, M. J. Devlin, S. M. Duff, A. J. Duivenvoorden, J. Dunkley, R. Dünner, P. A. Gallardo, Y. Guan, D. Han, J. C. Hill, G. C. Hilton, M. Hilton, R. Hložek, J. Hubmayr, K. M. Huffenberger, J. P. Hughes, B. J. Koopman, A. MacInnis, J. McMahon, M. S. Madhavacheril, K. Moodley, T. Mroczkowski, S. Naess, F. Nati, L. B. Newburgh, M. D. Niemack, L. A. Page, B. Partridge, M. Salatino, N. Sehgal, A. Schillaci, C. Sifón, K. M. Smith, D. N. Spergel, S. Staggs, E. R. Storer, H. Trac, J. N. Ullom, J. Van Lanen, L. R. Vale, A. van Engelen, M. V. Magaña, E. M. Vavagiakis, E. J. Wollack, Z. Xu, and Atacama Cosmology Telescope Collaboration, Atacama Cosmology Telescope: Combined kinematic and thermal Sunyaev-Zel'dovich measurements from BOSS CMASS and LOWZ halos, Phys. Rev. D **103**, 063513 (2021), arXiv:2009.05557 [astro-ph.CO].

[34] F. J. Qu, B. D. Sherwin, M. S. Madhavacheril, D. Han, K. T. Crowley, I. Abril-Cabezas, P. A. R. Ade, S. Aiola, T. Alford, M. Amiri, S. Amodeo, R. An, Z. Atkins, J. E. Austermann, N. Battaglia, E. S. Battistelli, J. A. Beall, R. Bean, B. Beringue, T. Bhandarkar, E. Biermann, B. Bolliet, J. R. Bond, H. Cai, E. Calabrese, V. Calafut, V. Capalbo, F. Carrero, J. Carron, A. Challinor, G. E. Chesmore, H.-m. Cho, S. K. Choi, S. E. Clark, R. Córdova Rosado, N. F. Cothard, K. Coughlin, W. Coulton, R. Dalal, O. Darwish, M. J. Devlin, S. Dicker, P. Doze, C. J. Duell, S. M. Duff, A. J. Duivenvoorden, J. Dunkley, R. Dünner, V. Fanfani, M. Fankhanel, G. Farren, S. Ferraro, R. Freundt, B. Fuzia, P. A. Gallardo, X. Garrido, V. Gluscevic, J. E. Golec, Y. Guan, M. Halpern, I. Harrison, M. Hasselfield, E. Healy, S. Henderson, B. Hensley, C. Hervías-Caimapo, J. C. Hill, G. C. Hilton, M. Hilton, A. D. Hincks, R. Hložek, S.-P. P. Ho, Z. B. Huber, J. Hubmayr, K. M. Huffenberger, J. P. Hughes, K. Irwin, G. Isopi, H. T. Jense, B. Keller, J. Kim, K. Knowles, B. J. Koopman, A. Kosowsky, D. Kramer, A. Kusiak, A. La Posta, A. Lague, V. Lakey, E. Lee, Z. Li, Y. Li, M. Limon, M. Lokken, T. Louis, M. Lungu, N. MacCrann, A. MacInnis, D. Maldonado, F. Maldonado, M. Mallaby-Kay, G. A. Marques, J. McMahon, Y. Mehta, F. Menanteau, K. Moodley, T. W. Morris, T. Mroczkowski, S. Naess, T. Namikawa, F. Nati, L. Newburgh, A. Nicola, M. D. Niemack, M. R. Nolta, J. Orlowski-Scherer, L. A. Page, S. Pandey, B. Partridge, H. Prince, R. Puddu, F. Radiconi, N. Robertson, F. Rojas, T. Sakuma, M. Salatino, E. Schaan, B. L. Schmitt, N. Sehgal, S. Shaikh, C. Sierra, J. Sievers, C. Sifón, S. Simon, R. Sonka, D. N. Spergel, S. T. Staggs, E. Storer, E. R. Switzer, N. Tampier, R. Thornton, H. Trac, J. Treu, C. Tucker, J. Ullom, L. R. Vale, A. Van Engelen, J. Van Lanen, J. van Marrewijk, C. Vargas, E. M. Vavagiakis, K. Wagoner, Y. Wang, L. Wenzl, E. J. Wollack, Z. Xu, F. Zago, and K. Zheng, The Atacama Cosmology Telescope: A Measurement of the DR6 CMB Lensing Power Spectrum and Its Implications for Structure Growth, ApJ **962**, 112 (2024), arXiv:2304.05202 [astro-ph.CO].

[35] N. Padmanabhan, X. Xu, D. J. Eisenstein, R. Scalzo, A. J. Cuesta, K. T. Mehta, and E. Kazin, A 2 per cent distance to z = 0.35 by reconstructing baryon acoustic oscillations - I. Methods and application to the Sloan Digital Sky Survey, MNRAS **427**, 2132 (2012), arXiv:1202.0090 [astro-ph.CO].

[36] D. J. Eisenstein, H.-J. Seo, E. Sirko, and D. N. Spergel, Improving Cosmological Distance Measurements by Reconstruction of the Baryon Acoustic Peak, ApJ **664**, 675 (2007), astro-ph/0604362.

[37] M. White, Reconstruction within the Zeldovich approximation, MNRAS **450**, 3822 (2015), arXiv:1504.03677 [astro-ph.CO].

[38] B. Ried Guachalla, E. Schaan, B. Hadzhiyska, and S. Ferraro, Velocity reconstruction in the era of DESI and Rubin/LSST. I. Exploring spectroscopic, photometric, and hybrid samples, Phys. Rev. D **109**, 103533 (2024), arXiv:2312.12435 [astro-ph.CO].

[39] S. Yuan, H. Zhang, A. J. Ross, J. Donald-McCann, B. Hadzhiyska, R. H. Wechsler, Z. Zheng, S. Alam, V. Gonzalez-Perez, J. N. Aguilar, S. Ahlen, D. Bianchi, D. Brooks, A. de la Macorra, K. Fanning, J. E. Forero-Romero, K. Honscheid, M. Ishak, R. Kehoe, J. Lasker, M. Landriau, M. Manera, P. Martini, A. Meisner, R. Miquel, J. Moustakas, S. Nadathur, J. A. Newman, J. Nie, W. Percival, C. Poppett, A. Rocher, G. Rossi, E. Sanchez, L. Samushia, M. Schubnell, H.-J. Seo, G. Tarlé, B. A. Weaver, J. Yu, Z. Zhou, and H. Zou, The DESI one-per cent survey: exploring the halo occupation distribution of luminous red galaxies and quasi-stellar objects with ABACUSSUMMIT, MNRAS **530**, 947 (2024), arXiv:2306.06314 [astro-ph.CO].

[40] B. Hadzhiyska, S. Ferraro, R. Pakmor, S. Bose, A. M. Delgado, C. Hernández-Aguayo, R. Kannan, V. Springel, S. D. M. White, and L. Hernquist, Interpreting Sunyaev-Zel'dovich observations with MillenniumTNG: mass and environment scaling relations, MNRAS **526**, 369 (2023), arXiv:2305.00992 [astro-ph.CO].

[41] D. Nelson, V. Springel, A. Pillepich, V. Rodriguez-Gomez, P. Torrey, S. Genel, M. Vogelsberger, R. Pakmor, F. Marinacci, R. Weinberger, L. Kelley, M. Lovell, B. Diemer, and L. Hernquist, The IllustrisTNG simulations: public data release, Computational Astrophysics and Cosmology **6**, 2 (2019), arXiv:1812.05609 [astro-ph.GA].

[42] D. Nelson, A. Pillepich, S. Genel, M. Vogelsberger, V. Springel, P. Torrey, V. Rodriguez-Gomez, D. Sijacki, G. F. Snyder, B. Griffen, F. Marinacci, L. Blecha, L. Sales, D. Xu, and L. Hernquist, The illustris simulation: Public data release, Astronomy and Computing **13**, 12 (2015), arXiv:1504.00362 [astro-ph.CO].

[43] G. Kauffmann, D. Nelson, S. Borthakur, T. Heckman, L. Hernquist, F. Marinacci, R. Pakmor, and A. Pillepich, The morphology and kinematics of the gaseous circumgalactic medium of Milky Way mass galaxies - II. Comparison of IllustrisTNG and Illustris simulation results, MNRAS **486**, 4686 (2019), arXiv:1904.07274 [astro-ph.GA].

[44] V. Rodriguez-Gomez, G. F. Snyder, J. M. Lotz, D. Nelson, A. Pillepich, V. Springel, S. Genel, R. Weinberger, S. Tacchella, R. Pakmor, P. Torrey, F. Marinacci, M. Vogelsberger, L. Hernquist, and D. A. Thilker, The optical morphologies of galaxies in the IllustrisTNG simulation: a comparison to Pan-STARRS observations, MNRAS **483**, 4140 (2019), arXiv:1809.08239 [astro-ph.GA].

[45] A. Amon and G. Efstathiou, A non-linear solution to the S_8 tension?, MNRAS **516**, 5355 (2022), arXiv:2206.11794 [astro-ph.CO].

[46] A. S. Maniyar, S. Ferraro, and E. Schaan, Doppler Boosted Dust Emission and Cosmic Infrared Background–Galaxy Cross-Correlations: A New Probe of Cosmology and Astrophysics, Phys. Rev. Lett. **130**, 041001 (2023), arXiv:2204.05299 [astro-ph.CO].

[47] A. Kusiak, B. Bolliet, S. Ferraro, J. C. Hill, and A. Krolewski, Constraining the baryon abundance with the kinematic Sunyaev-Zel'dovich effect: Projected-field detection using P l a n c k , W M A P , and u n W I S E, Phys. Rev. D **104**, 043518 (2021), arXiv:2102.01068 [astro-ph.CO].

[48] J. Chaves-Montero, C. Hernández-Monteagudo, R. E. Angulo, and J. D. Emberson, Measuring the evolution of intergalactic gas from z = 0 to 5 using the kinematic Sunyaev-Zel'dovich effect, MNRAS **503**, 1798 (2021), arXiv:1911.10690 [astro-ph.CO].

[49] M. Mallaby-Kay, S. Amodeo, J. C. Hill, M. Aguena, S. Allam, O. Alves, J. Annis, N. Battaglia, E. S. Battistelli, E. J. Baxter, K. Bechtol, M. R. Becker, E. Bertin, J. R. Bond, D. Brooks, E. Calabrese, A. Carnero Rosell, M. Carrasco Kind, J. Carretero, A. Choi, M. Crocce, L. N. da Costa, M. E. S. Pereira, J. De Vicente, S. Desai, J. P. Dietrich, P. Doel, C. Doux, A. Drlica-Wagner, J. Dunkley, J. Elvin-Poole, S. Everett, S. Ferraro, I. Ferrero, J. Frieman, P. A. Gallardo, J. García-Bellido, G. Giannini, D. Gruen, R. A. Gruendl, G. Gutierrez, S. R. Hinton, D. L. Hollowood, D. J. James, A. Kosowsky, K. Kuehn, M. Lokken, T. Louis, J. L. Marshall, J. McMahon, J. Mena-Fernández, F. Menanteau, R. Miquel, K. Moodley, T. Mroczkowski, S. Naess, M. D. Niemack, R. L. C. Ogando, L. Page, S. Pandey, A. Pieres, A. A. Plazas Malagón, M. Raveri, M. Rodriguez-Monroy, E. S. Rykoff, S. Samuroff, E. Sanchez, E. Schaan, I. Sevilla-Noarbe, E. Sheldon, C. Sifón, M. Smith, M. Soares-Santos, F. Sobreira, E. Suchyta, G. Tarle, C. To, C. Vargas, E. M. Vavagiakis, N. Weaverdyck, J. Weller, P. Wiseman, and B. Yanny, Kinematic Sunyaev-Zel'dovich effect with ACT, DES, and BOSS: A novel hybrid estimator, Phys. Rev. D **108**, 023516 (2023), arXiv:2305.06792 [astro-ph.CO].

[50] B. Bolliet, J. Colin Hill, S. Ferraro, A. Kusiak, and A. Krolewski, Projected-field kinetic Sunyaev-Zel'dovich Cross-correlations: halo model and forecasts, J. Cosmology Astropart. Phys. **2023**, 039 (2023), arXiv:2208.07847 [astro-ph.CO].

[51] T. Mroczkowski, P. A. Gallardo, M. Timpe, A. Kiselev, M. Groh, H. Kaercher, M. Reichert, C. Cicone, R. Puddu, P. Dubois-dit-Bonclaude, D. Bok, E. Dahl, M. Macintosh, S. Dicker, I. Viole, S. Sartori, G. Andrés Valenzuela Venegas, M. Zeyringer, M. Niemack, S. Poppi, R. Olguin, E. Hatziminaoglou, C. De Breuck, P. Klaassen, F. Montenegro-Montes, and T. Zimmerer, Design of the 50-meter Atacama Large Aperture Submm Telescope, arXiv e-prints , arXiv:2402.18645 (2024), arXiv:2402.18645 [astro-ph.IM].

[52] L. Di Mascolo, Y. Perrott, T. Mroczkowski, S. Andreon, S. Ettori, A. Simionescu, S. Raghunathan, J. van Marrewijk, C. Cicone, M. Lee, D. Nelson, L. Sommovigo, M. Booth, P. Klaassen, P. Andreani, M. A. Cordiner, D. Johnstone, E. van Kampen, D. Liu, T. J. Maccarone, T. W. Morris, A. Saintonge, M. Smith, A. E. Thelen, and S. Wedemeyer, Atacama Large Aperture Submillimeter Telescope (AtLAST) Science: Resolving the Hot and Ionized Universe through the Sunyaev-Zeldovich effect, arXiv e-prints , arXiv:2403.00909 (2024), arXiv:2403.00909 [astro-ph.CO].

[53] S. Amodeo, N. Battaglia, E. Schaan, S. Ferraro, E. Moser, S. Aiola, J. E. Austermann, J. A. Beall, R. Bean, D. T. Becker, R. J. Bond, E. Calabrese, V. Calafut, S. K. Choi, E. V. Denison, M. Devlin, S. M. Duff, A. J. Duivenvoorden, J. Dunkley, R. Dünner, P. A. Gallardo, K. R. Hall, D. Han, J. C. Hill, G. C. Hilton, M. Hilton, R. Hložek, J. Hubmayr, K. M. Huffenberger, J. P. Hughes, B. J. Koopman, A. MacInnis, J. McMahon, M. S. Madhavacheril, K. Moodley, T. Mroczkowski, S. Naess, F. Nati, L. B. Newburgh, M. D. Niemack, L. A. Page, B. Partridge, A. Schillaci, N. Sehgal, C. Sifón, D. N. Spergel, S. Staggs, E. R. Storer, J. N. Ullom, L. R. Vale, A. van Engelen, J. Van Lanen, E. M. Vavagiakis, E. J. Wollack, and Z. Xu, Atacama Cosmology Telescope: Modeling the gas thermodynamics in BOSS CMASS galaxies from kinematic and thermal Sunyaev-Zel'dovich measurements, Phys. Rev. D **103**, 063514 (2021),

arXiv:2009.05558 [astro-ph.CO].

[54] E. Moser, N. Battaglia, D. Nagai, E. Lau, L. F. Machado Poletti Valle, F. Villaescusa-Navarro, S. Amodeo, D. Anglés-Alcázar, G. L. Bryan, R. Dave, L. Hernquist, and M. Vogelsberger, The Circumgalactic Medium from the CAMELS Simulations: Forecasting Constraints on Feedback Processes from Future Sunyaev-Zeldovich Observations, ApJ **933**, 133 (2022), arXiv:2201.02708 [astro-ph.CO].

[55] C. Preston, A. Amon, and G. Efstathiou, A non-linear solution to the S_8 tension - II. Analysis of DES Year 3 cosmic shear, MNRAS **525**, 5554 (2023), arXiv:2305.09827 [astro-ph.CO].

[56] L. Bigwood, A. Amon, A. Schneider, J. Salcido, I. G. McCarthy, C. Preston, D. Sanchez, D. Sijacki, E. Schaan, S. Ferraro, N. Battaglia, A. Chen, S. Dodelson, A. Roodman, A. Pieres, A. Ferte, A. Alarcon, A. Drlica-Wagner, A. Choi, A. Navarro-Alsina, A. Campos, A. J. Ross, A. Carnero Rosell, B. Yin, B. Yanny, C. Sanchez, C. Chang, C. Davis, C. Doux, D. Gruen, E. S. Rykoff, E. M. Huff, E. Sheldon, F. Tarsitano, F. Andrade-Oliveira, G. M. Bernstein, G. Giannini, H. T. Diehl, H. Huang, I. Harrison, I. Sevilla-Noarbe, I. Tutusaus, J. Elvin-Poole, J. McCullough, J. Zuntz, J. Blazek, J. DeRose, J. Cordero, J. Prat, J. Myles, K. Eckert, K. Bechtol, K. Herner, L. F. Secco, M. Gatti, M. Raveri, M. Carrasco Kind, M. R. Becker, M. A. Troxel, M. Jarvis, N. MacCrann, O. Friedrich, O. Alves, P. F. Leget, R. Chen, R. P. Rollins, R. H. Wechsler, R. A. Gruendl, R. Cawthon, S. Allam, S. L. Bridle, S. Pandey, S. Everett, T. Shin, W. G. Hartley, X. Fang, Y. Zhang, M. Aguena, J. Annis, D. Bacon, E. Bertin, S. Bocquet, D. Brooks, J. Carretero, F. J. Castander, L. N. da Costa, M. E. S. Pereira, J. De Vicente, S. Desai, P. Doel, I. Ferrero, B. Flaugher, J. Frieman, J. Garcia-Bellido, E. Gaztanaga, G. Gutierrez, S. R. Hinton, D. L. Hollowood, K. Honscheid, D. Huterer, D. J. James, K. Kuehn, O. Lahav, S. Lee, J. L. Marshall, J. Mena-Fernandez, R. Miquel, J. Muir, M. Paterno, A. A. Plazas Malagon, A. Porredon, A. K. Romer, S. Samuroff, E. Sanchez, D. Sanchez Cid, M. Smith, M. Soares-Santos, E. Suchyta, M. E. C. Swanson, G. Tarle, C. To, N. Weaverdyck, J. Weller, P. Wiseman, and M. Yamamoto, Weak lensing combined with the kinetic Sunyaev Zel'dovich effect: A study of baryonic feedback, arXiv e-prints , arXiv:2404.06098 (2024), arXiv:2404.06098 [astro-ph.CO].